AD-A152 991 RESTRIKE PARTICLE BEAM EXPERIMENTS ON A DENSE PLASMA FOCUS OPENING SWITCH..(U) ILLINOIS UNIV AT URBANA FUSION STUDIES LAB G GERDIN JUN 85 FSL-181 1/1

UNCLASSIFIED AFOSR-TR-85-0279 AFOSR-79-0121 F/G 20/8 NL

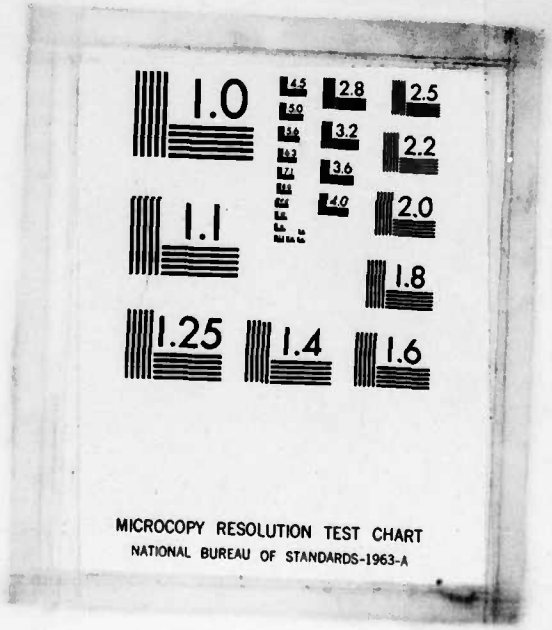
1.0
1.1
1.25
1.4
1.6
1.8
2.0
2.2
2.5
2.8
3.2
3.6
4.0
4.5
5.0
5.6
6.3
MICROCOPY RESOLUTION TEST CHART
NATIONAL BUREAU OF STANDARDS-1963-A

AFOSR-TR- 85-0279

(2)

FSL-181

Final Report
30 Sept. 1979 - 29 Sept. 1984

Restrike Particle Beam Experiments on a Dense Plasma Focus

30 Sept. 1979 - May 1982

U.I. FUSION STUDIES LABORATORY
Nuclear Engineering Program
University of Illinois
Urbana, Illinois 61801

2

FSL-181

Final Report
30 Sept. 1979 - 29 Sept. 1984

Restrike Particle Beam Experiments on a Dense Plasma Focus
30 Sept. 1979 - May 1982

Opening Switch Research on a Dense Plasma Focus
May 1982 - 30 Sept. 1984

Glenn Gerdin
Fusion Studies Laboratory
Nuclear Engineering Program
University of Illinois
Urabana, Illinois 61801

June 1985

Accession For	
NTIS GRA&I	☒
DTIC TAB	☐
Unannounced	☐
Justification	
By	
Distribution/	
Availability Codes	
Dist	Avail and/or Special
A-1	

UNCLASSIFIED

SECURITY CLASSIFICATION OF THIS PAGE (When Data Entered)

REPORT DOCUMENTATION PAGE	READ INSTRUCTIONS BEFORE COMPLETING FORM
1. REPORT NUMBER AFOSR-TR- 85-0279 FSL-181	2. GOVT ACCESSION NO. / 3. RECIPIENT'S CATALOG NUMBER
4. TITLE (and Subtitle) Restrike Particle Beam Experiments on a Dense Plasma Focus, 30 Sept. 1979 - May 1982 Opening Switch Research on a Plasma Focus - May 1982 - 29 Sept. 1984	5. TYPE OF REPORT & PERIOD COVERED Final Report 30 Sept. 1979 - 29 Sept. 1984 / 6. PERFORMING ORG. REPORT NUMBER
7. AUTHOR(s) Glenn Gerdin	8. CONTRACT OR GRANT NUMBER(s) [redacted]-AFOSR-79-0121
9. PERFORMING ORGANIZATION NAME AND ADDRESS Nuclear Engineering Program 214 Nuclear Engineering Lab. 103 S. Goodwin Ave., Urbana, IL 61801	10. PROGRAM ELEMENT, PROJECT, TASK AREA & WORK UNIT NUMBERS 61102F 2301/A7
11. CONTROLLING OFFICE NAME AND ADDRESS Air Force Office of Scientific Research Building 410, Bolling AFB, DC 20332	12. REPORT DATE Jan. 25, 1985 / 13. NUMBER OF PAGES
14. MONITORING AGENCY NAME & ADDRESS (if different from Controlling Office) Same as above	15. SECURITY CLASS. (of this report) Unclassified / 15a. DECLASSIFICATION/DOWNGRADING SCHEDULE

16. DISTRIBUTION STATEMENT (of this Report)

Approved for public release; distribution unlimited

17. DISTRIBUTION STATEMENT (of the abstract entered in Block 20, if different from Report)

Same as above

18. SUPPLEMENTARY NOTES

19. KEY WORDS (Continue on reverse side if necessary and identify by block number)

cont'd

Dense Plasma Focus,
Particle Beam Generation,
Opening Switch,
Load Experiments,
Pulsed Power,

20. ABSTRACT (Continue on reverse side if necessary and identify by block number)

(over)

DD FORM 1 JAN 73 1473 EDITION OF 1 NOV 65 IS OBSOLETE S/N 0102-014-6601

UNCLASSIFIED

SECURITY CLASSIFICATION OF THIS PAGE (When Data Entered)

Abstract: Final Report

Grant # USAF-AFOSR-79-0121

Research on this grant has focused on plasma focus experiments in the areas of particle beam generation and as a potential repetitive opening switch.

In pursuing the former unique diagnostic tools were developed to measure the scaling of particle beam current and energy for both the electron and ion beams generated by the device. Simultaneous measurements of the energy spectra for both the electrons and ion beams were measured for the first time as were scaling laws for the increase of electron energy and current with input energy.

The potential of the plasma focus as an opening switch was then investigated. Measurements of the current and voltage waveforms indicated that the resistance of the pinch was roughly ten times the classical value which was estimated from electron temperature measurements and streak pictures. Load experiments were performed with 100MW being delivered to a 0.77 ohm load with a pulse compression factor of 10 and a transfer efficiency of $2 \cdot 10^{-3}$. To increase the efficiency the impaler concept was devised which could have a transfer effi of well over 50% according to the results of a physical model. The frequency of the microwave emission was measured using the delay line technique. The observed frequencies were most consistent with the lower hybrid frequency. A model is being devised to explain this emission and the enhanced pinch resistance.

cont keywords include: 001473

Final Report for AFOSR

Grant# USAF-AFOSR-79-0121

1979-82 Restrike Beam Experiments on a Dense Plasma Focus

1982-84 Opening Switch Research on a Plasma Focus

I. 30 Sept. 1979 to May 1982: Restrike Beam Experiment

The goal of the research at the beginning of the funding period was to determine the nature of the particle beams generated by a dense plasma focus. This research was performed between 30 Sept. 1979 and May 1982 when results of the beam-target model for neutron production generated by deuteron beams were presented at the IEEE Conference in Ottawa, Canada.[1] In the course of this research unique diagnostic tools were developed to study these particle beams including a differentially pumped Faraday cup to measure ion energies by time of flight,[2] a solid state nuclear track detector technique to measure high fluences of light ions,[3] an electron magnetic spectrometer,[4] and[2] filtered electron Faraday cup.[4] These and other diagnostic tools were used to measure the energy spectra and intensity of the electron and ion beams generated by a plasma focus and the scaling of these beams with input energy. The results were the first of their kind and are well summarized in detail in our publication in Nuclear Fusion[5] which is included here as an appendix.

While the scaling laws indicated a hardening (increased particle energy) and intensifying of the particle beams with input energy, the broad spread of particle energies (power law distributions) seemed to limit the application of such an accelerator (although the electron beam may have promise in microwave generation[6] or as a pump for lasing media.[7]). At the same time it became apparent that the strong current interruption in the plasma focus might make it a good candidate as an opening switch.

good candidate as an opening switch.

II. May 1982 to 20 Sept. 1982

This research began after meeting Prof. Schoenbach at the 3rd Pulsed Power Conference in Albuquerque, NM in June 1981. After having had several telephone conversations with him since that meeting it was realized that the possibility of a sucessful collaboration existed. This was strongly encouraged by the grant monitor at that time, Lt. Col. A. K. Hyder, so in January 1982, G. Gerdin (principle investigator on this grant) traveled to Texas Tech University for a three day visit to discuss the possible nature of this collaboration.

Prof. Schoenbach is an ideal man with whom to collaborate since he had been involved with dense plasma focus (DPF) research for about ten years and is the author of over ten papers on the subject. Presently he is directing a project on diffuse dischage opening switches and so has experience in both DPF and opening switch physics.

A previous unsuccessful attempt to use the plasma focus as an opening switch[8] was regarded as not a true test of a plasma focus as an opening switch. That is, it did not appear the device had been operated in an optimum manner since no capacitive discharge data showing strong interruptions were presented[9] and the initial $\dot{I}_o$ was very low.[9] Furthermore the circuit used[9] represented a brute force approach and the results indicated a more sophisticated circuit or gas handling technique would be required. So a research program was devised to provide experimental tests to gain an understanding of the DPF interruption physics under ideal conditions of a capacitive energy drive and static gas fill.

The research program devised on this trip was to answer these four basic questions:

a) Is the interruption inductive ($\dot{L}$) or resistive in nature?

b) Can the power be tapped into a load?

c) Can the timing of the interruption be controlled?

c) Can the operation be made repetitive.

To answer the first question it is important to know the nature of the resistivity of the plasma (classical or anomalous?). To determine whether the plasma exhibits classical resistivity[10] or not one must know the electron temperature. A soft-x-ray spectrometer was developed[11] during May-October 1982 which utilized pin diodes and Ross filters [12-15] for fast time response. Also a computer program was developed[11] using a steady state corona model.

The results show good consistency, yielding temperatures of about 0.3 to 0.5 keV, regardless of the type of impurity gas present (neon or nitrogen; Figure 1). This result is encouraging since most of the detected x-ray emission from a nitrogen seeded plasma, is of the continum type, as opposed to a neon seeded plasma where line radiation dominates the detected emission. Roughly the same temperatures are expected in both cases, given the small amount of impurity gas present (about 2%). Strong pinches were observed with pure neon as the working gas (0.6 torr) and with temperatures about the same as reported above.

It was also possible to calculate the classical (Spitzer) resistance of the pinch from evaluated dimension of the x-ray image of the pinch. This is roughly 9 mΩ at a temperature of 500 eV. This value is about fifty times lower than the observed 0.5Ω value (from current interruption measurements) suggesting the possibility of non-classical (anomalous) resistivity playing an important role in the focus current interruption at pinch time.

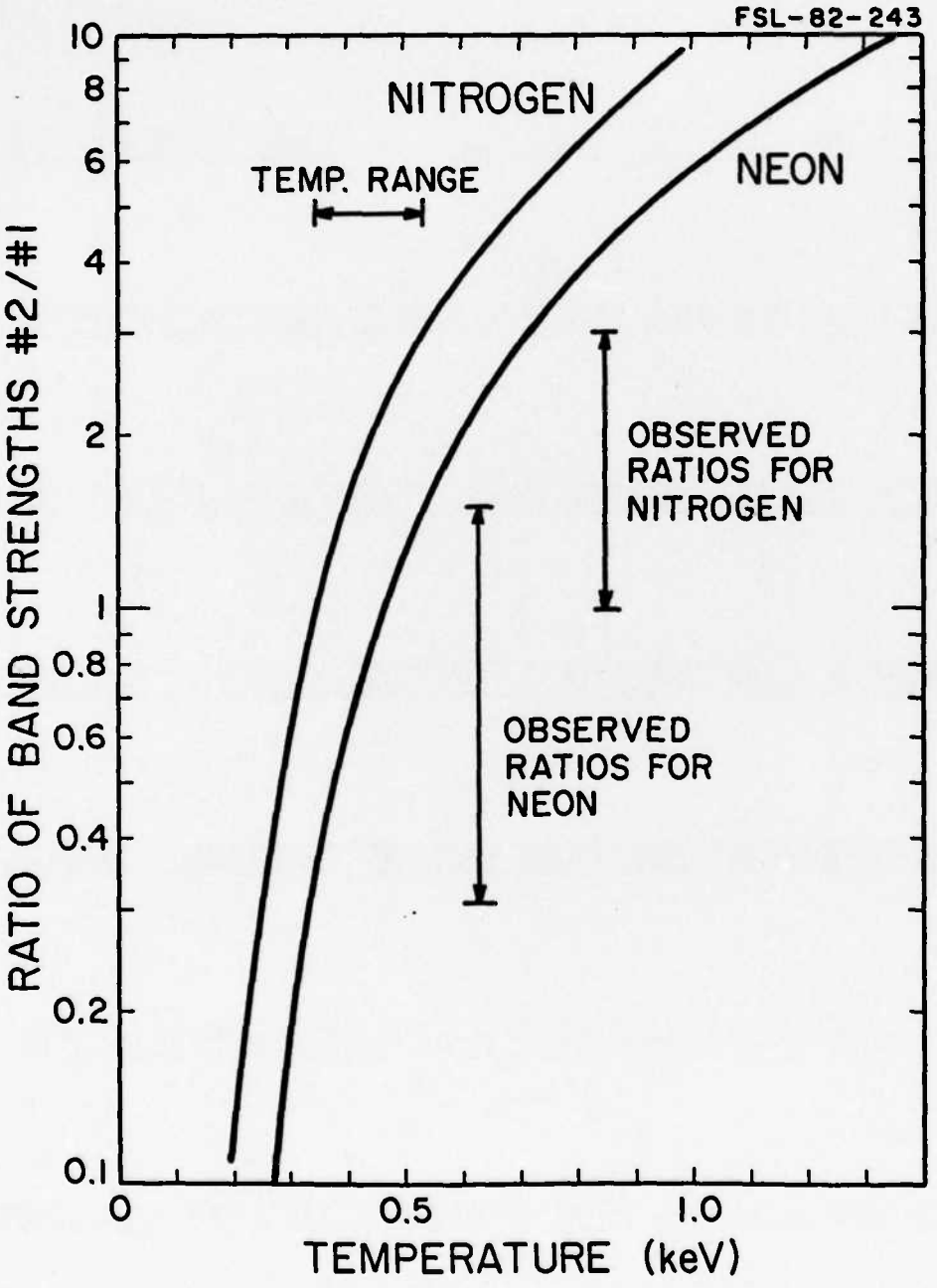

Figure 1. Ratio of band strengths vs. temperature, as determined by computer simulation (corona model) for deuterium fills with 2% nitrogen and 2% neon.

III. 30 Sept. 1982 - 30 Sept. 1983: Opening Switch Research on a Plasma Focus

During this period the research effort on the plasma focus as an opening switch benefited greatly by the collaboration with the pulsed power group at the Texas Tech University. This collaboration took the form of a winter visit by Professors Schoenbach and Krompholz to the University of Illinois to plan the preparations for Professor Krompholz's more extended visit in June. During his visit experiments involving microwave emission, pinch phenomena through streak pictures and the Mark I load experiments were performed.

The research could be divided into three phases:

1) Development and testing of a O•D model describing the motion of the current sheaths in a dense plasma focus.
2) Observation of the phenomena occurring at pinch time with normal operating procedures.
3) Performing DPF load-coupling experiments.

The O•D model developed was a combination of a couple of others[2,3] and was found to be in good agreement with observations of the motion of the current sheath in the pre-pinch stage.[4] The model predicted that the pinch would bounce radially and result in a rapid voltage reversal across the load and a loss of power flow. This prediction was tested by the experiments of phase 2 and phase 3.

Phase 2 of the experiments was the major activity during the first two weeks of Prof. Krompholz's visit. These experiments consited of the following:

1) Observation of the time behavior of the microwave emission over various frequency bands.
2) The use of radial and axial streak camera pictures to observe phenomena at pinch time to test some of the conclusions from phase 1.

3) Taking soft-xray pinhole camera pictures simultaneously with the axial streak picture to get a more comprehensive view of the pinch phenomena.

Microwave emission was observed simply by placing microwave horns and detectors in the room outside the device. Emission was observed to be coming from between the parallel plates. The period of duration of the emission gets shorter as the frequency of the band is increased (Figure 2) with the highest frequency emission occuring just after pinch time. This could be consistent with an emission frequency proportional to the local magnetic field (e.g. the lower hybrid) frequency or density such as the ion plasma frequency. The magnitude of the emission frequency is most consistent with the lower hybrid for conditions believed to be present in the discharge during this period (see next section). Since the lower hybrid instability is associated with anomalous resistivity this could prove to be an extremely interesting result.

The radial streak pictures provided a test as to whether the radial bounce predicted by the 0•D code actually occurred. The experiments with a streak camera set up to observe the radial implosion of the pinch (Figure 3) confirmed the presence of this bounce; the effect of the bounce limiting the power flow to the load was confirmed by the results of the load coupling experiments.[19]

Axial streak pictures (Figures 4, 5) revealed that the first compression involves an approximately uniform compression of the plasma column but that second compression involves local constrictions of the column indicating the onset of mhd instabilities (usually kinks). Comparison with the current waveform of the DPF (Figure 5) indicates that the maximum device current interruption occurs during 1st compression.

Thus, the conclusions resulting from phase 2 of the experiments were that the radial bounce occurs and is detrimental to efficiency energy transfer and

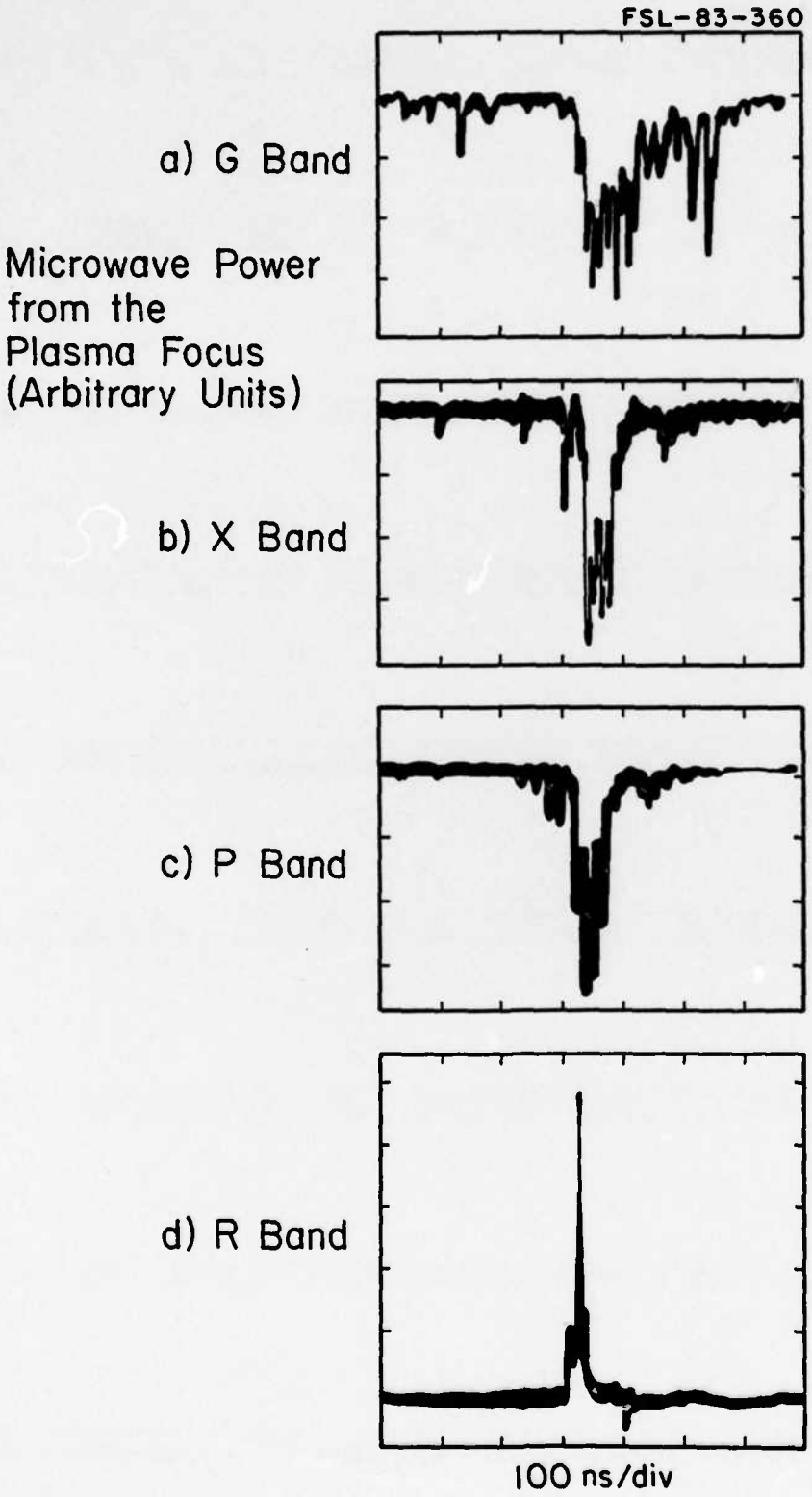

Figure 2. Typical microwave power generated by the Illinois plasma focus (not the same shot) as observed with a horn-detector and oscilloscope over the following frequency bands: 1) G band (4-6 GHz), 2) X band (8-12 GHz), 3) P band (12.4-18 GHz), and 4) R band (26.5-40 GHz).

FSL-83-339

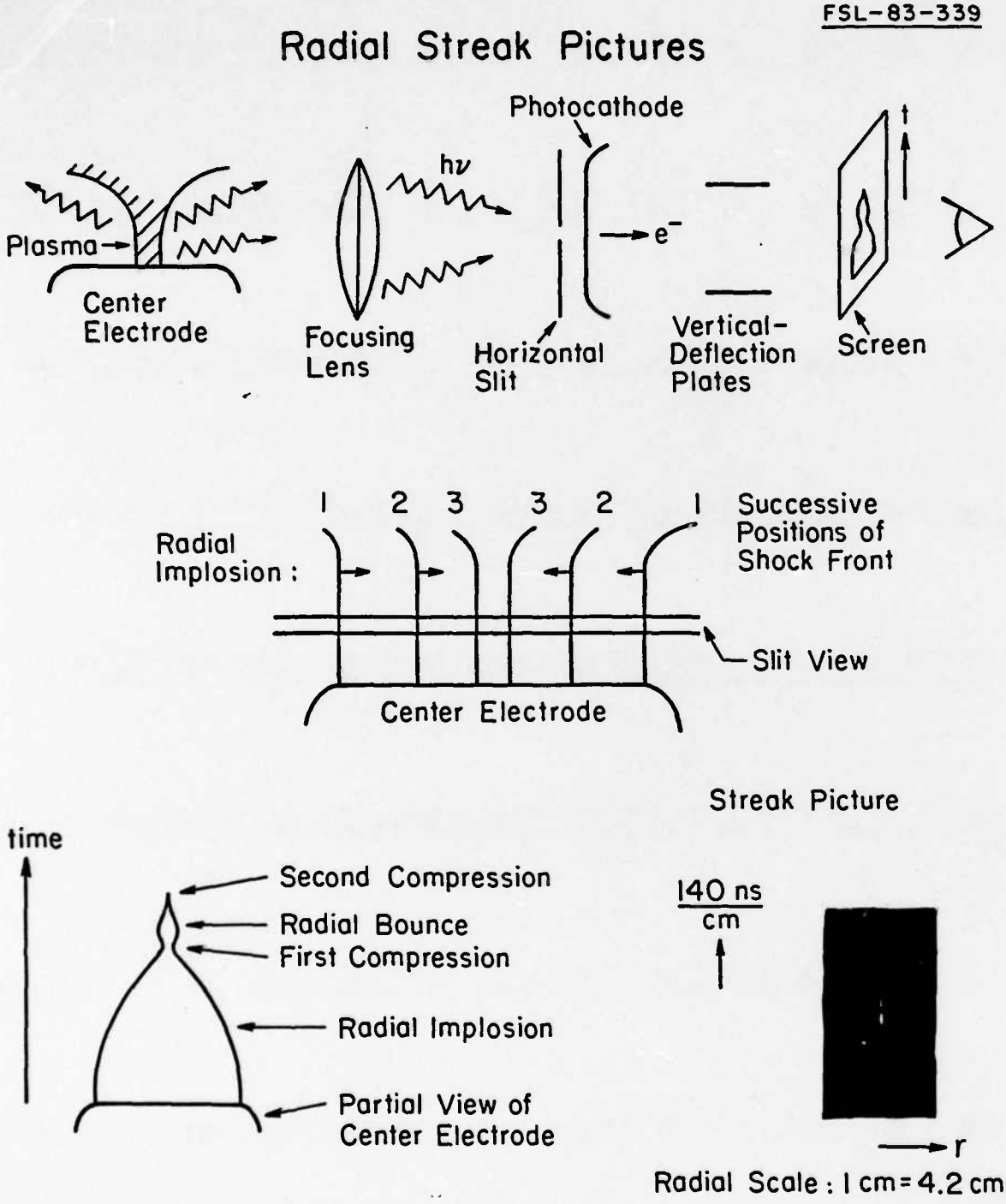

Figure 3. Top: A schematic of the plasma and streak camera in the radial streak configuration.
Middle: Camera view of the plasma at three successive instants of time.
Bottom: An interpretation of the radial streak picture and an actual photograph.

FSL-83-340

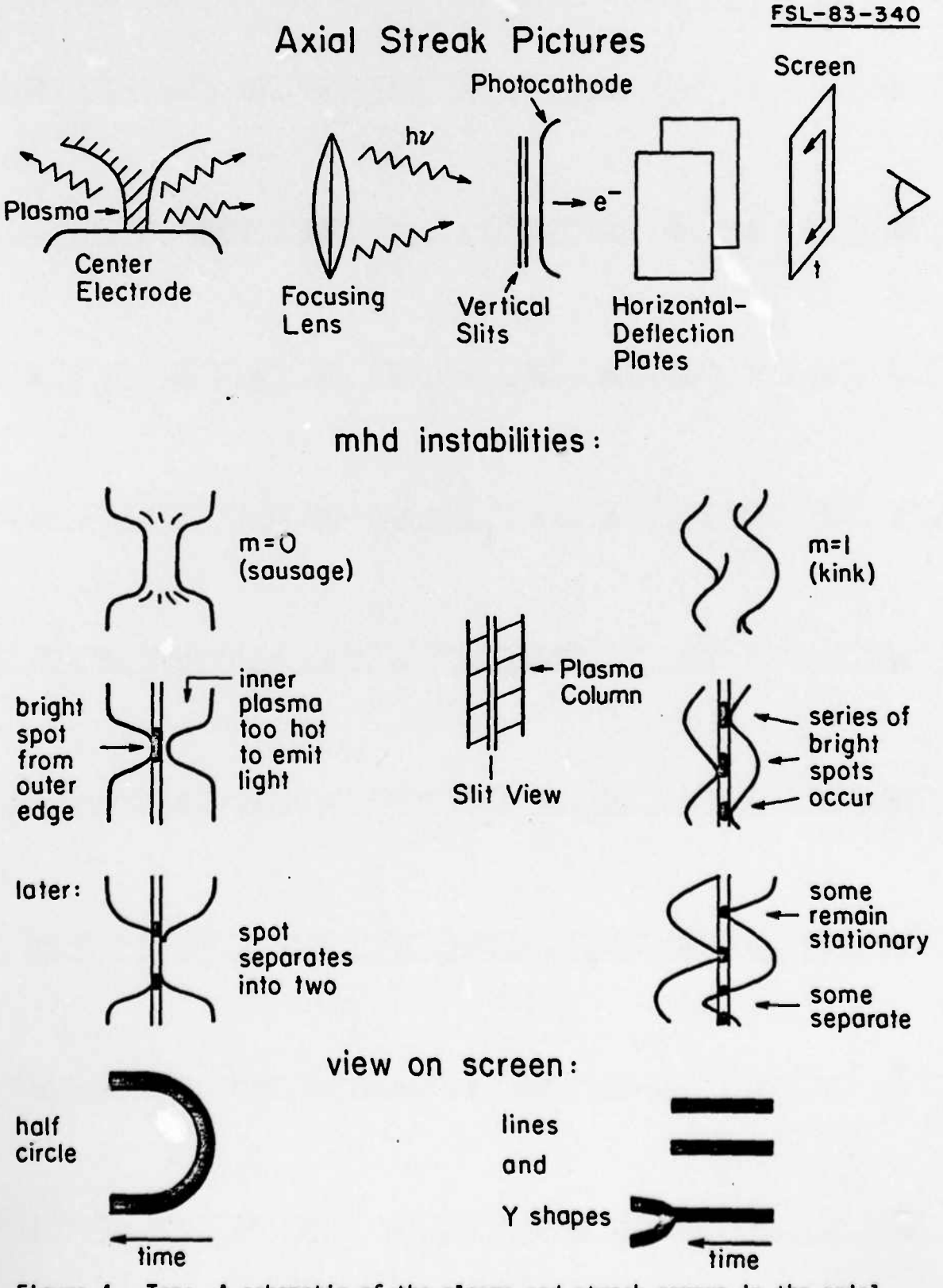

Figure 4. Top: A schematic of the plasma and streak camera in the axial configuration. Middle: Various possible macroscopic or mhd instabilities that could occur. Bottom: The appearance on the screen if either type instability (sausage or kink) were to occur.

FSL-83-341

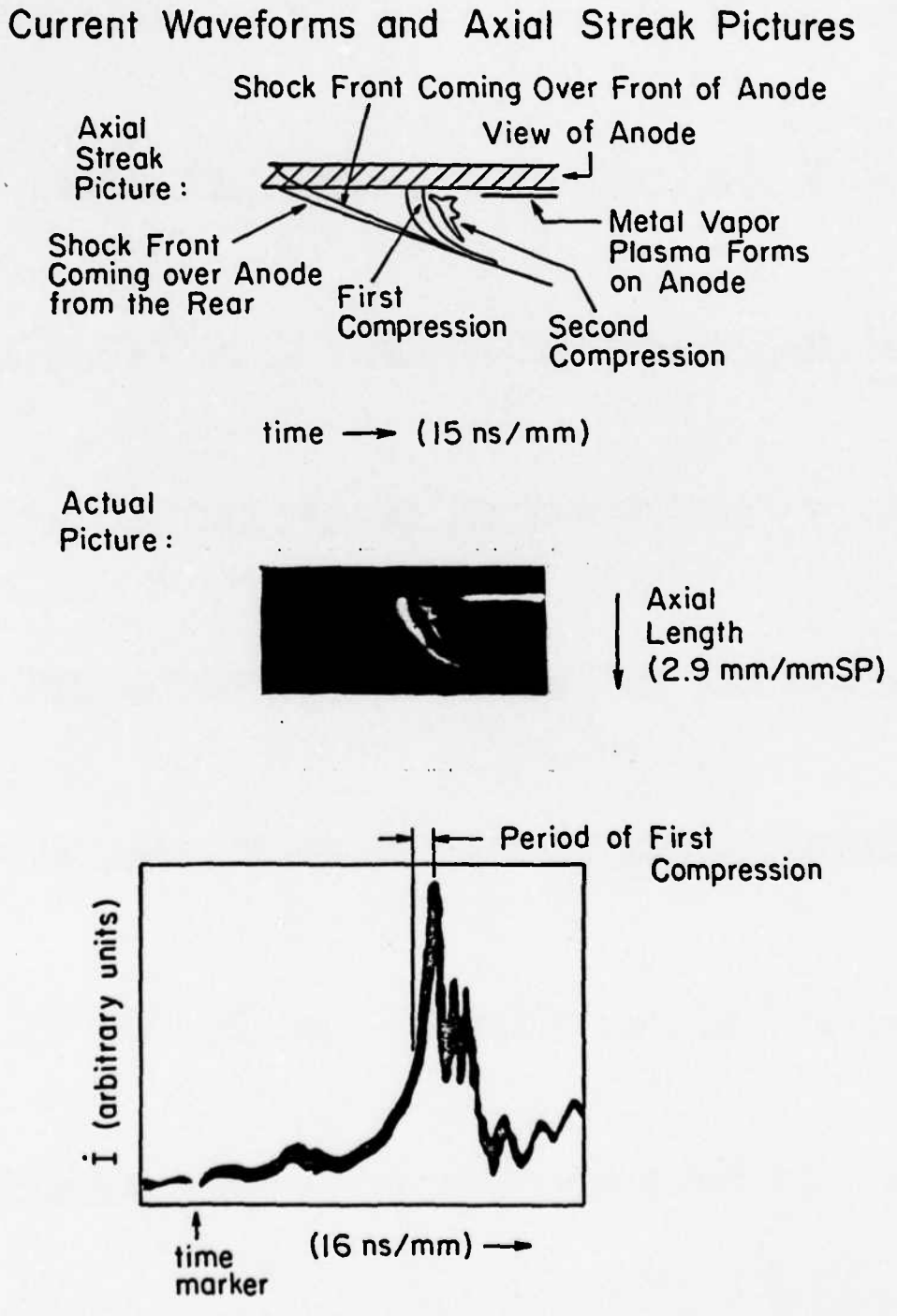

Figure 5. Comparison of an axial streak picture with the time derivative of the device current. The peak in the current interruption occurs during first compression.

that first compression is the most important phase of energy transfer. Thus, reducing the effects of the instabilities and enhancing the effects of the first compression appear to be the keys to improving efficiency.

The DPF load coupling experiments (phase 3) tended to confirm the results of phase 2. The load was hooked up to the DPF across the breach end of the device. The results are shown in Table. I. Coupling efficiency appears limited by rapid oscillations in load voltage (Figure 6) which appear to be caused by the radial bounce and subsequent mhd activity during 2nd compression (Figure 5). The voltage across the load at the breach end of the DPF is consistent with the 0-D computer model.[18]

One strategy to improve the coupling efficiency including the addition of an axial magnetic field to stabilize the column to enhance first compression and prevent mhd instabilities.[12] The addition of an axial magnetic filed has been previously found[12] to affect the discharge as follows:

1) Stabilize the plasma column to mhd instabilities

2) Increase the duration of current interruption

3) Decrease the magnitude of the rate of current interruption.

The first result is consistent with classical mhd theory[20] and the last two have been confirmed by the results of preliminary experiments on the Illinois DPF.[19] The third result implies a reduced load voltage which hurts coupling efficiency and thus must be considered as a trade-off in the design of an optimal energy coupling device.

In conclusion the results of the FY 1982-83 research on this project have supplied at least partial answers to the first two questions listed in the research objectives sections of this report. That is the current interruption is both resistive and inductive in nature as evidenced by partial reversal of

TABLE 1

	Mark II	Impaler
Bank Capacitance, C	40μF	40μF
Bank Voltage, V_o	25kV	25kV
Bank Energy, E_o	12.5kJ	12.5kJ
Plasma Current, I	560kA	560kA
Load Inductance, L_ℓ	30nH	26nH
Load Resistance, R_ℓ	0.77Ω	0.77Ω
Time to Interruption,	1.75μs	1.75μs
Period of Interruption, T	200ns	100ns
Peak Load Current, I_ℓ	11kA	250kA
Peak Power to Load, P_ℓ	100MW	63GW
Peak Load Voltage, V_ℓ	17.5kV	250kV
Energy Transfer, E_ℓ	25J	6.3kJ
Transfer Efficiency, η	$2 \cdot 10^{-3}$	50%

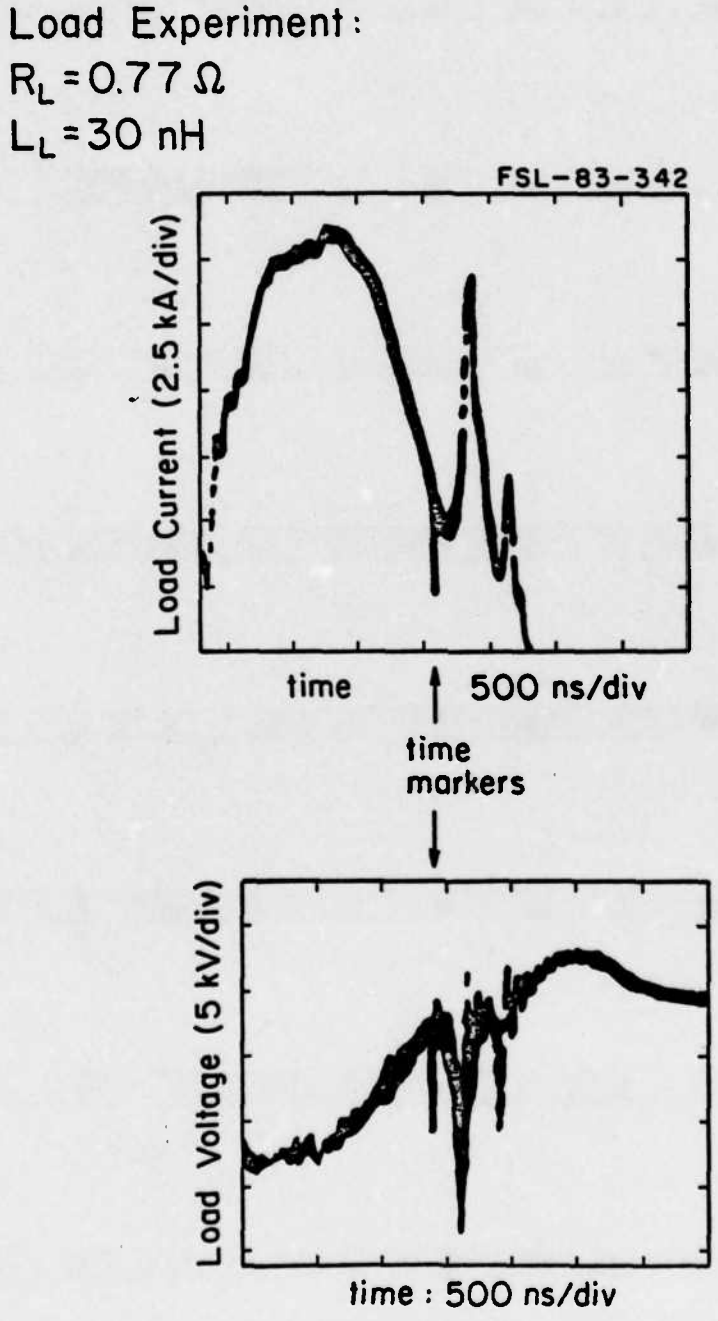

Figure 6. Experimental results from the Mark II load coupling experiment (Table I) with a configuration similar to Figure 5 except that load switch S_2 was closed at all times; hence the occurrence of load current before pinch time. The energy transferred during the first sharp load voltage spike was 27 J.

load voltage due to the radial bounce which is an inductive effect. Also power can be tapped into a load but enhancing the efficiency to an interesting power transfer device will probably involve strategies to increase the resistive nature and suppress the inductive nature ($\dot{IL}$) of the device.

IV. 30 Sept. 1983 to 30 Sept. 1984

A) Research Objectives

In the previous year, 100 MW was coupled into a load but the efficiency (energy delivered to the initial capacitor bank energy) was only 0.2%. Thus the research centered on discovering ways to greatly enhance this efficiency. To achieve this, a two pronged approach was formulated: one, to try to understand the nature of the current interruption in the plasma focus; and two, to use circuit analysis and preliminary measurements to design a potentially more efficient configuration for testing. The progress made in achieving these goals is presented in the next section.

B) Status of the Research Effort

The research performed in the past fiscal year involved the detailed study of microwave emission by the device and the design of a muzzle-end load coupling experiment to enhance the voltage delivered to the load. Since the microwave emission is orders of magnitude above thermal levels,[21] it is an indication of microturbulence[22] and perhaps enhanced resistivity[23]. If the latter can be monitored and controlled, it could provide the basis for a high power opening switch. Muzzle-end load coupling is predicted[24] to increase the load voltage by a factor of five greater than the 25kV breach voltage pulse we observe. Since the power to resistive and hence transmission line loads is proportional to the square of this voltage, the system efficiency may be increased by a factor of twenty five. The progress in the muzzle-end coupling research and the results

of the microwave emission experiments will be discussed in the next two sections respectively.

B.1 Muzzle-end Coupling research: the Impaler Concept

This work consisted of two phases: the first involving preliminary experiments and the second, involving the coupling apparatus, was designed and constructed. Preliminary measurement of the coupling efficiency will be made in January 1985.

To get an idea of the nature of the potentials in the muzzle end of the device a floating Langmuir probe was inserted along the two lines labeled z and r in Figure 7. Since the impedance of the floating probe is kept high, the probe acquired a potential equivalent to that of a muzzle-end coupling electrode before it starts to draw significant current. Hence the floating potential, which is below[25] the true plasma potential by $3.87 \cdot KT_e/e$ for a deuterium plasma (~-100V in the current sheath ~-1 kV in the pinch), is really the quantity of interest for load coupling.

The results are shown in Figure 8 and typical waveforms in Figure 9. They are somewhat disappointing in that in no case is the floating potential greater than the breach voltage in spite of the predictions of the model. Either the high potential region is very localized on the axis and missed by the probe (the probe was bent when placed on the axis and hence the measurement of that point is unreliable) or the model is not valid.

The muzzel-end coupling device was then designed to test these results in a practical manner and to test a novel second approach to current interruption which we call the impaler concept.

The impaler concept is to achieve a current interruption by 'impaling' the current sheath on a ridged insulator as shown in Figure 10. This configuration

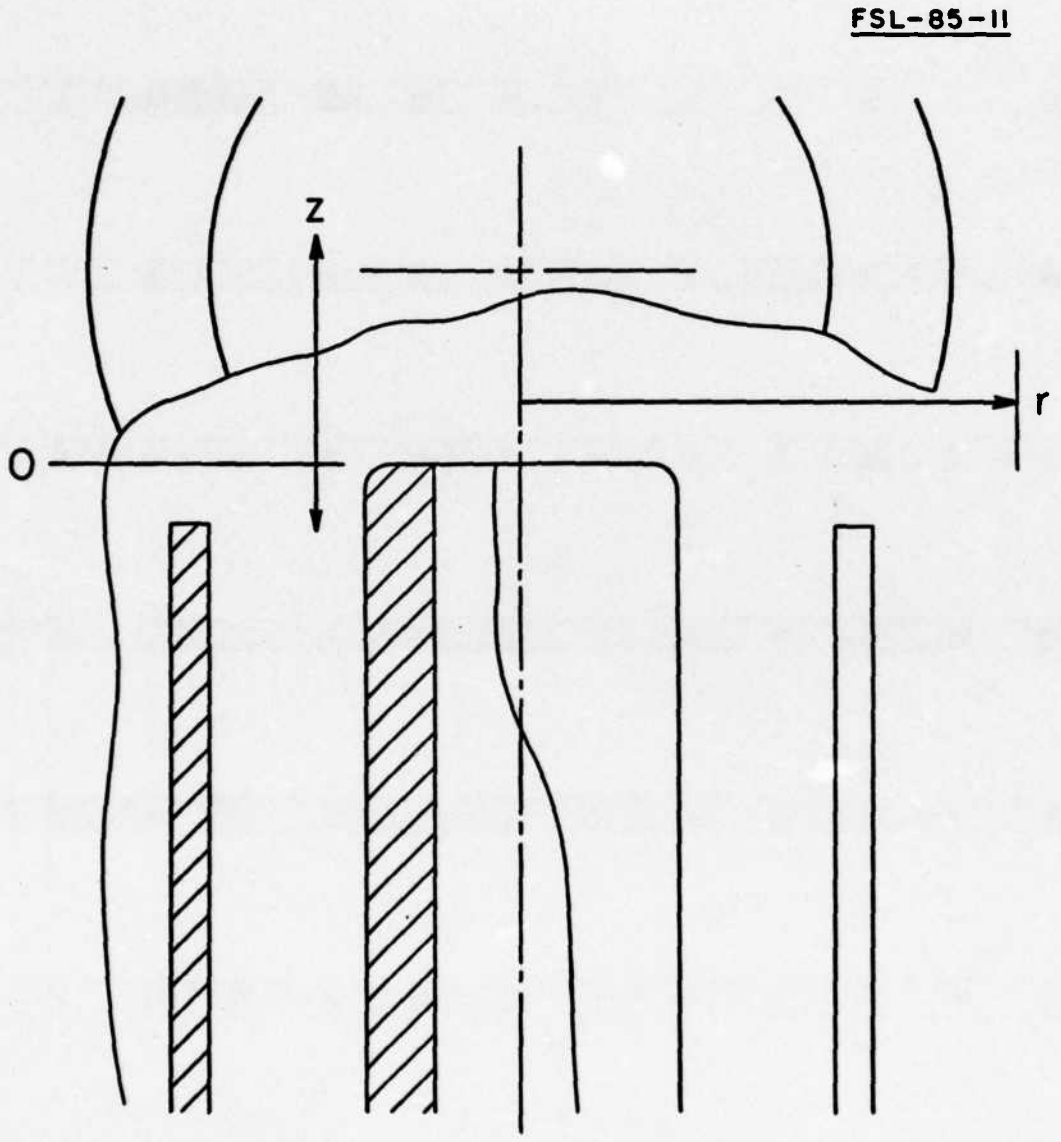

Figure 7. The relation of the vertical (z) and radial (r) tracks of the floating probe tip with respect to the inner and outer electrodes of the plasma focus. The results are shown in Figures 8 and 9.

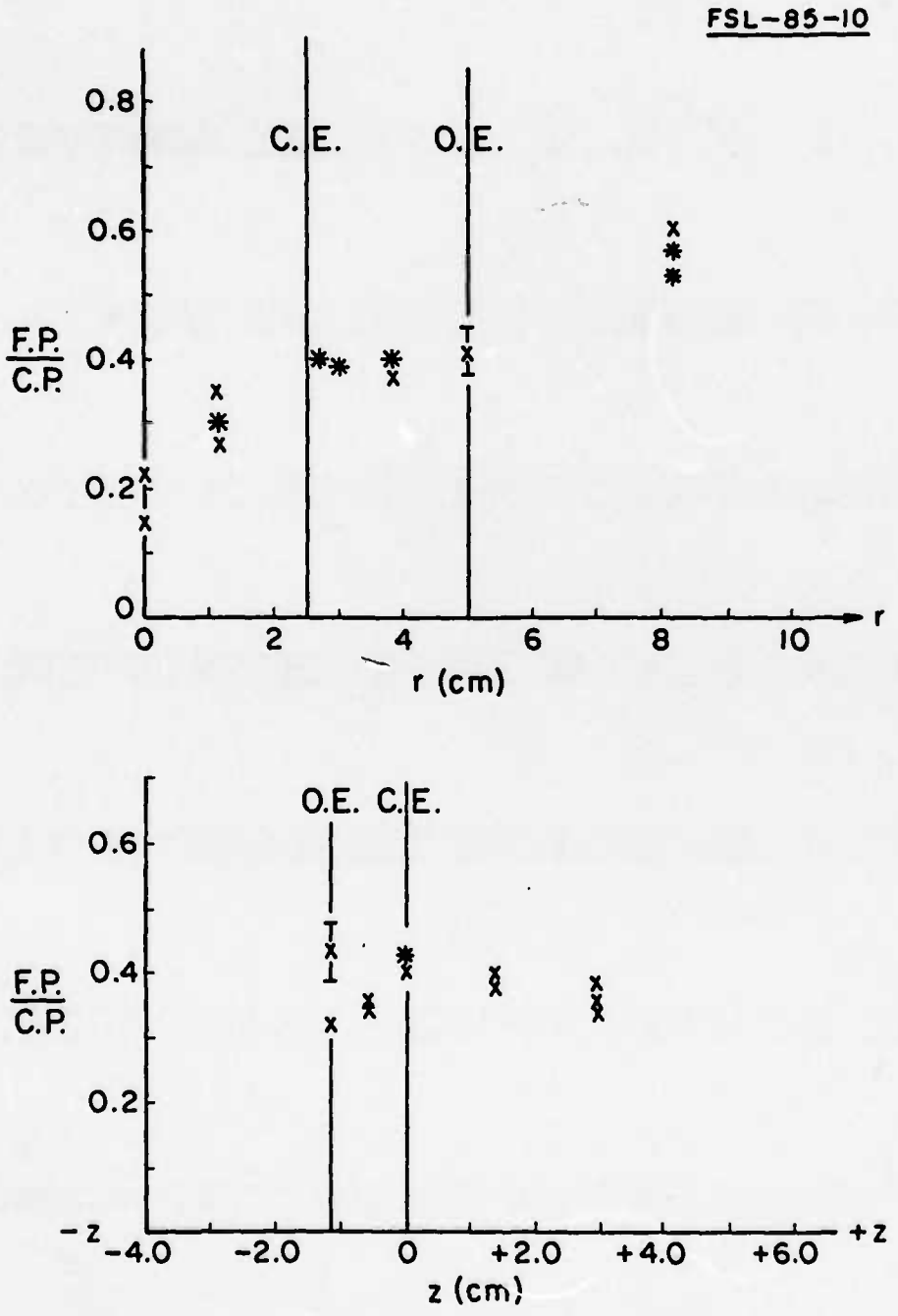

Figure 8. The ratio of the peak in the floating potential (F.P.) to the peak in the breach voltage (C.P.) as measured along the r and z tracks shown in Figure 7. Along the r tract (top) the radial positions of the outer edge of the center electrode (C.E.) and the inner edge of the outer electrode (O.E.) are shown. Similarly the position of the tops of the outer and center electrodes are indicated along the z track (bottom).

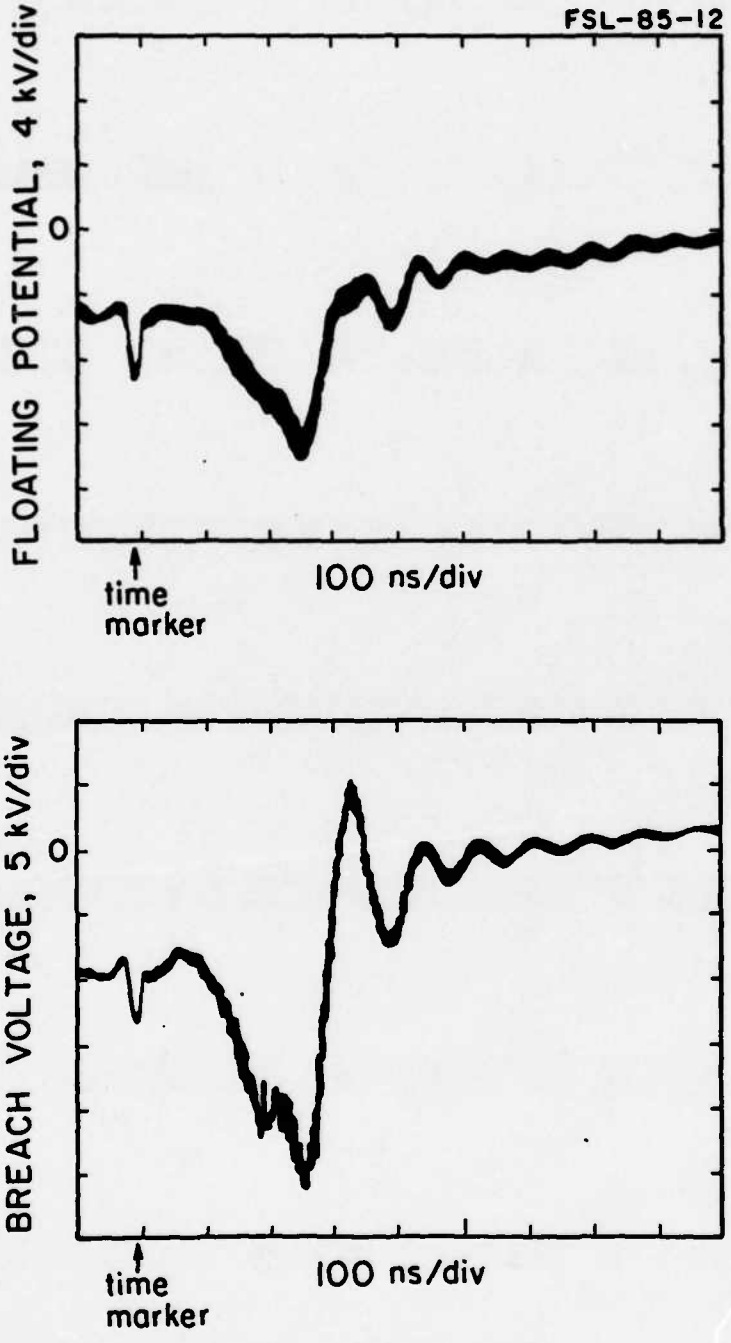

Figure 9. Typical simultaneous waveforms of the floating potential and breach voltage. The top of the floating probe was at a radial position of 5.1 cm (r track, Figure 7).

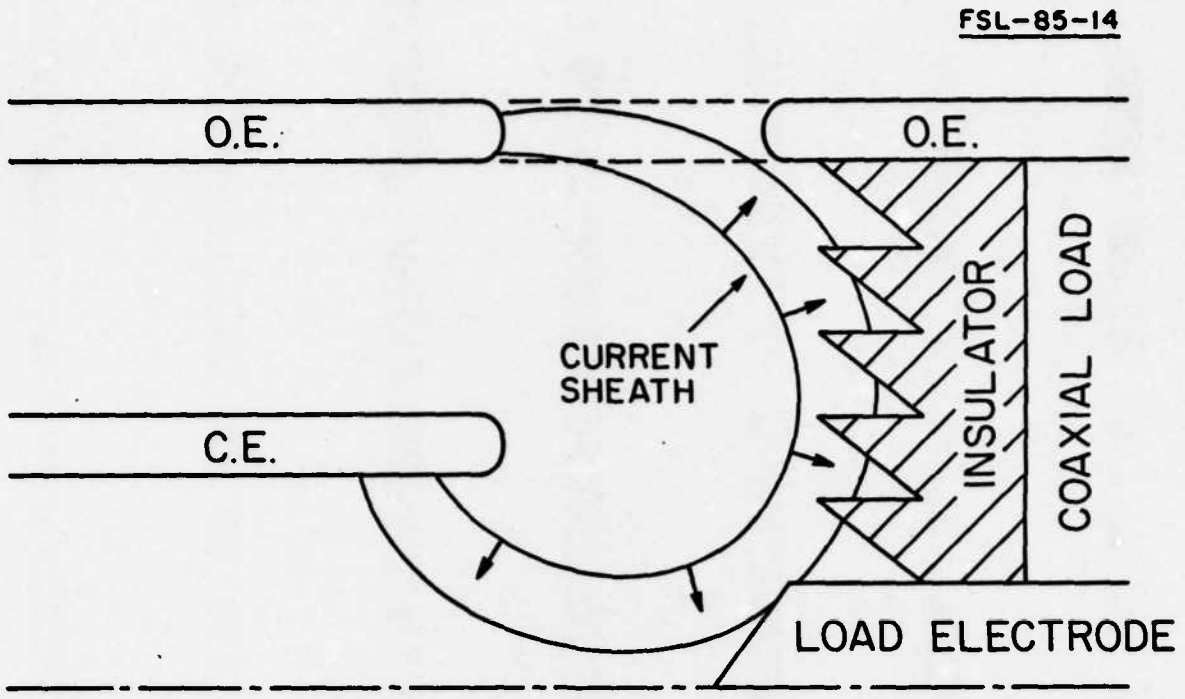

Figure 10. The impaler concept is illustrated. The current sheath being pushed to the right by its magnetic pressure impales itself on the jagged insulator which interrupts the current flow between the center (C.E.) and outer (O.E.) electrodes. By adjusting the length of the load electrode it should be possible for the current sheath itself to provide the connection between the center and load electrodes which is represented by the switch S_2 in Figure 11.

utilizes the continuation of the motion of the current sheath from the rundown phase to drive the interruption. The plasma itself provides the load switch connection S_2 in the opening switch circuit (Figure 11) and by adjusting the relative positions of the load electrode and the impaler insulator, it should be possible for the load connection and the current interruption to be made simultaneously. Thus prepulses on the load may be effectively eliminated. To study muzzle-end coupling the focus without the impaler effect one just has to place the impaler insulator further away from the plasma focus electrodes with respect to the load electrode. Then the pinch occurs before the impaling of the current sheath takes place.

The scaling laws for the impaler concept are quite favorable and are based on the better understood rundown phase of the plasma focus discharge.[12] The interruption time, T, should be equal to the thickness of the current sheath, ℓ_s, divided by its speed v_s. For plasma focus devices this speed is given by:[16]

$$v_s = \left(\frac{R^2}{2\mu_o \rho_o} \right)^{1/2} \qquad (1)$$

where ρ_o is the mass density of the filling gas. Thus the voltage generated by interruption, V_ℓ, is :

$$V_\ell = L_G \dot{I} \simeq L_G I \, v_s/\ell_s \qquad (2)$$

where L_G and I are the gun inductance and the device current respectively. For values measured in our experiment[18] ($\ell_s \sim 1$cm, $v_s \sim 10^7$cm/sec, $L_G \sim 50$nH, and I~500kA), T and V_ℓ are 10^{-7} sec and 250 kV respectively. For resistive loads (and hence long transmission line loads) the power transfer, P_ℓ, is V_ℓ^2/R_ℓ, where R_ℓ is the load resistance. Therefore, P_ℓ is given by:

$$P_\ell = \frac{V_\ell^2}{R_\ell} \sim \frac{(L_G I \, v_s/\ell_s)^2}{R_\ell} \propto \frac{L_G^2 I^4}{p R_\ell \ell_s^2} \qquad (3)$$

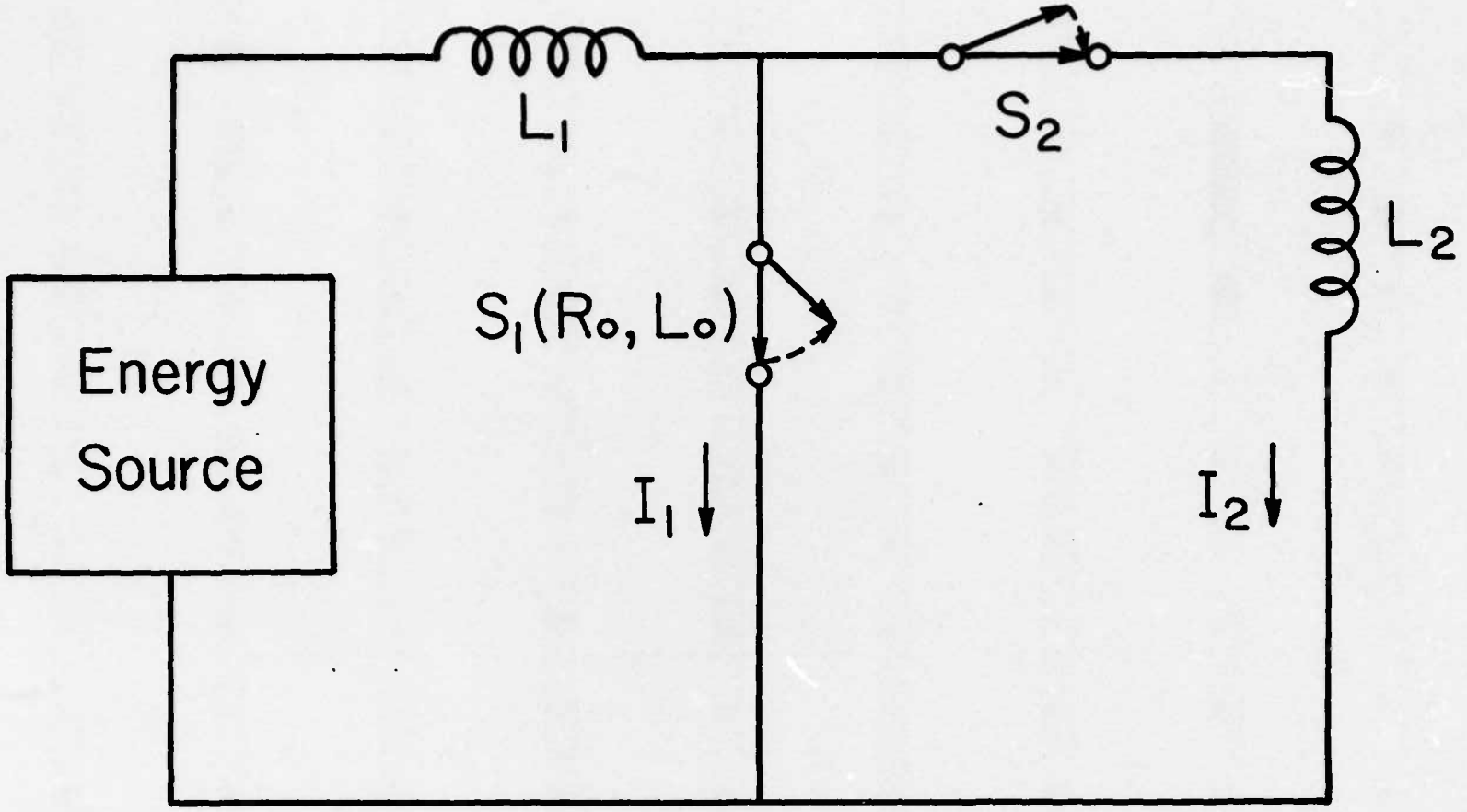

Figure 11. Basic source-load configuration for an inductive energy storage system where L_1 is the storage inductor and S_1 is the opening switch.

where p is the original pressure of the fill gas. The energy to the load, E_ℓ, is then given by:

$$E_\ell \sim P_\ell T = \frac{L_G^2 I^2}{R_\ell} \frac{v_s}{\ell_s} \propto \frac{L_G I^2}{R_\ell} \frac{L_G I}{p^{1/2} \ell_s} \qquad (4)$$

The system efficiency, η, them scales as:

$$\eta = E_\ell / E_o = \frac{L_G I^2}{1/2 L_G I^2} \frac{L_G v_s}{R_\ell \ell_s} = \frac{2 L_G v_s}{R_\ell \ell_s} \qquad (5)$$

or

$$\eta \propto \frac{2 L_G I}{R_\ell p^{1/2} \ell_s} \qquad (6)$$

The parameters for our present experiment are shown in Table I along with our previous load coupling results.

The improvement in performance is incredible. If the sheath thickness doesn't change with bank current one might be able to achieve a transfer efficiency of one into a resistive load at a device current of 1.1 MA. Such currents are relatively common in other plasma focus devices and we could even achieve this value in our present device with present facilities (although the spark gaps would have to be configured).

While this analysis has been based on several assumptions, the fact that the current's own magnetic pressure drives the current interruption makes the concept promising. The impaler electrodes have been constructed and the experiments in the coming months could be very interesting.

B.2 Microwave Emission

Due to the possible relationship between the generation of microwave radiation and turbulence induced resistivity of the plasma, the nature of the microwave emission was studied in detail to test various models for these phenomena.

The emission model is being formulated on the basis of various emission experiments which generally fall into three categories. They are as follows:

A). Measurement of source location and source strength for various microwave bands

B). Measurement of the frequency of the highest (and shortest duration) of emitted signal by the time-of-flight spectorscopy.

C). Time sequencing of the emission with various phenomenon that characterize a plasma focus discharge.

In the following three subsections each of these experiments will be discussed as to the nature of the measurement and the results. On the basis of the results of experiments (continuing) model will be selected in the fourth subsection.

B.2.1 Microwave source location and source strength

Microwave emission was observed by placing microwave horns and detectors outside the device. This is consistent with the observation from the DPF devices at Darmstadt[21] and Stevens Institute.[26] The power levels are on the order of ~1 mW for the R band (21 to 40 GHz) (or an intensity of 0.1 W/m^2) and somewhat higher for P, X, and G bands (Figure 2); the emission occurs during pinch time when the current is being interrupted. The emission is polarized in the direction of the normal of the parallel plates of the capcitor bank.[27]

The source of the microwave emission may be determined by changing the locations of the horns between shots and noting the change in signal strength. From these experiments, the microwaves appear to be emitted from between the plates of the parallel plates of the transmission lines and capacitor banks; the strength in the R band (21 to 40 GHz) is roughly uniform with position. This suggests that the plates are acting as antennas and transmission lines as opposed to waveguides. This possibility is strongly supported by the observation of emission in the G (4-6 GHz) and X bands (8-12 GHz) during periods when shorter wavelength emission in the P band (12-18 GHz) and the R band did not occur. The cutoff for the parallel plates of the capacitor banks (if they were to act like waveguides) is 14 GHz and no emission in the G and X bands should be observed.

To obtain more information on the location of the microwave source an R-band detector was attached to the anode so that it could view the region between the inner and outer electrode directly (Figure 12). The waveguide was aligned so the electric field vector for its $TE_{1,0}$ mode is parallel to the radial vector of the coaxial electrodes. The intensity level measured was typically over 600 W/m^2 and occured during the interruption in current (Figure 13). This intensity is almost 10^4 higher than that measured outside the device. Since the waveguide was pointed toward the muzzle end of the coaxial electrodes (Figure 12) this is strong evidence that the source region can be restricted to muzzle end of the device.

B.2.2 The measurement of the frequency of the R-band emission

Microwave radiation in the R-band is typically 30 to 50 ns in duration and contains several peaks each with a width of less than five nanoseconds (Figure14). The narrowness of the peaks makes it possible to measure the fre-

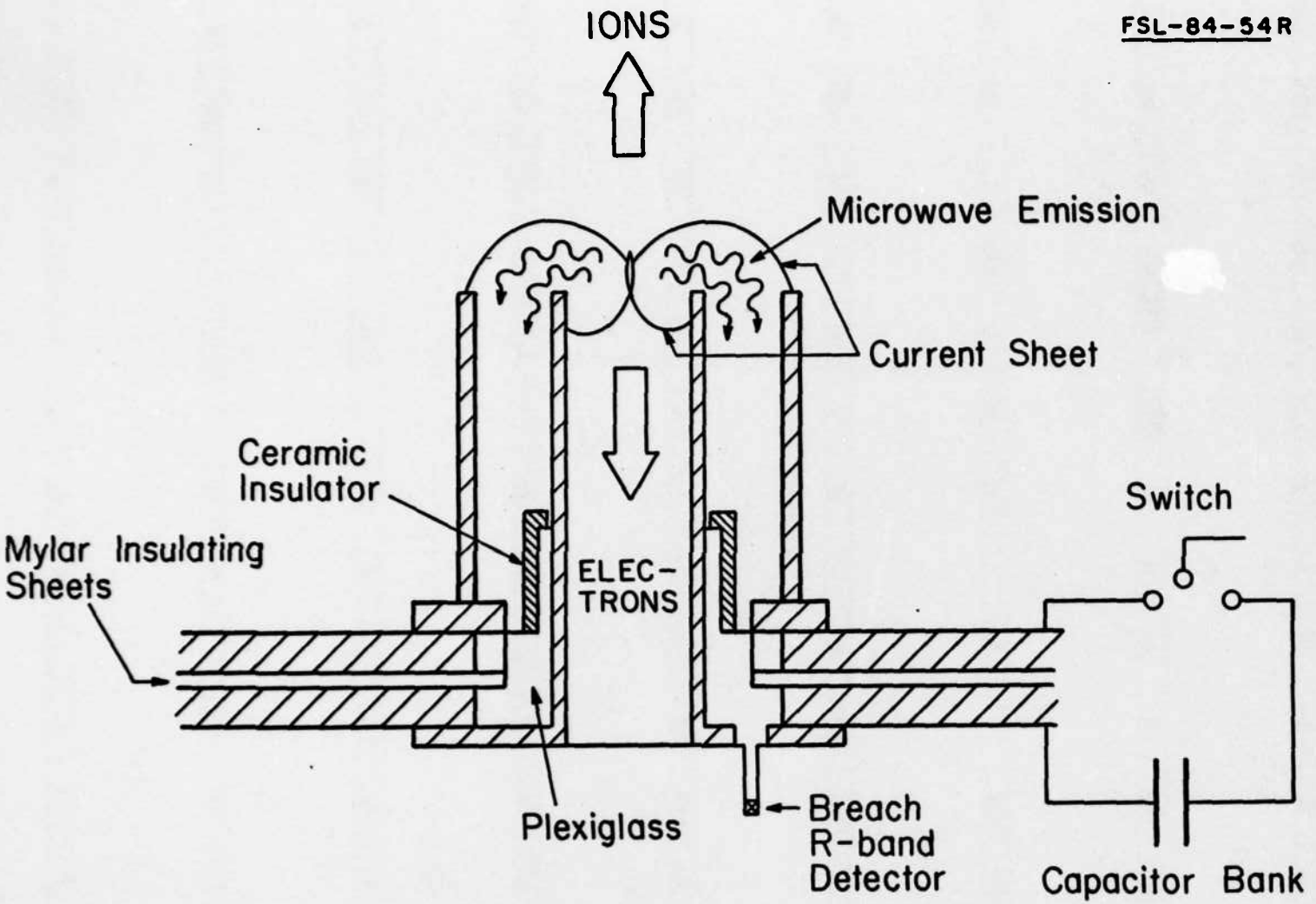

Figure 12. Schematic of the Mather-type DPF used at the University of Illinois. Microwave radiation is emitted from the Mylar insulating sheets placed between the parallel plate transmission line. The radiation originates in or near the focused plasma and propagates between the coaxial electrodes. Also shown is the location of the R band detector used in the measurements of the microwave intensity in the breach end of the device.

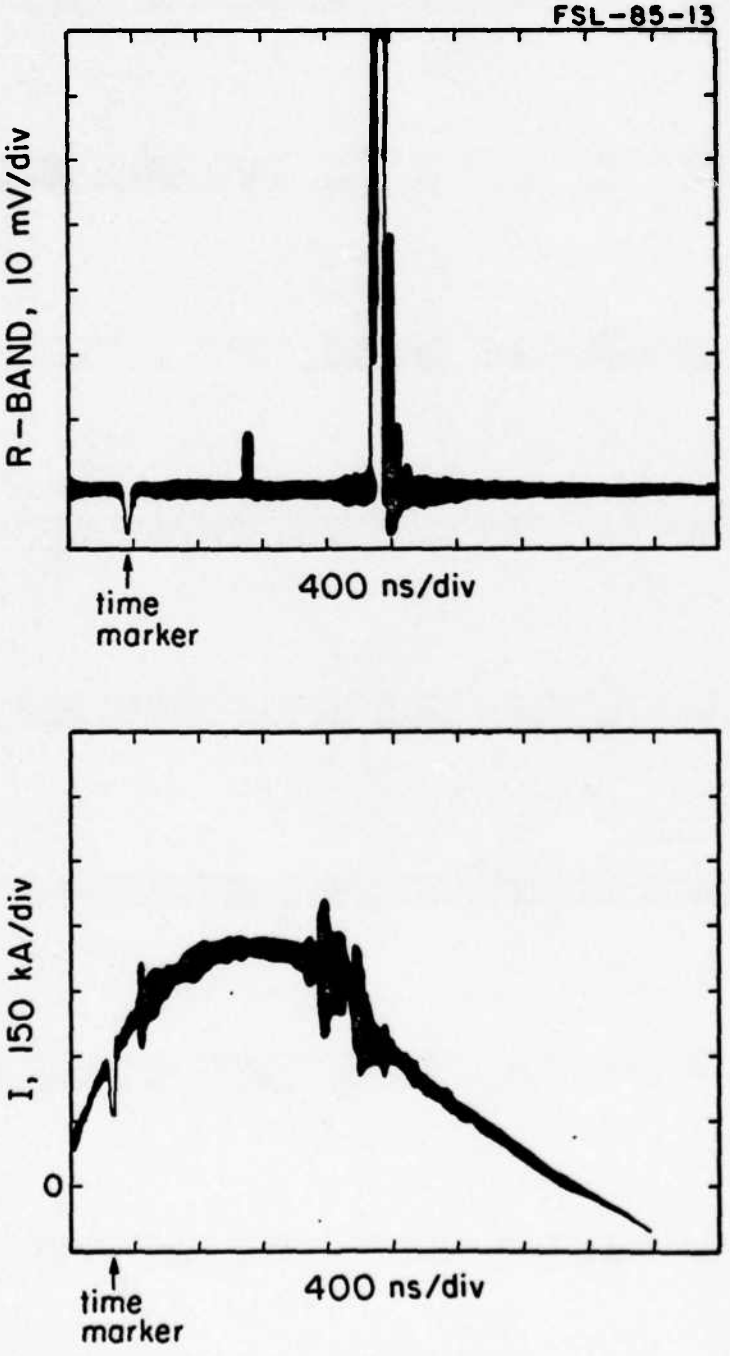

Figure 13. Typical waveforms for the breach emission of microwaves in the R band. Also shown is a current waveform which shows the emission occurs near the end of the current interruption as consistent with previous measurements.[19]

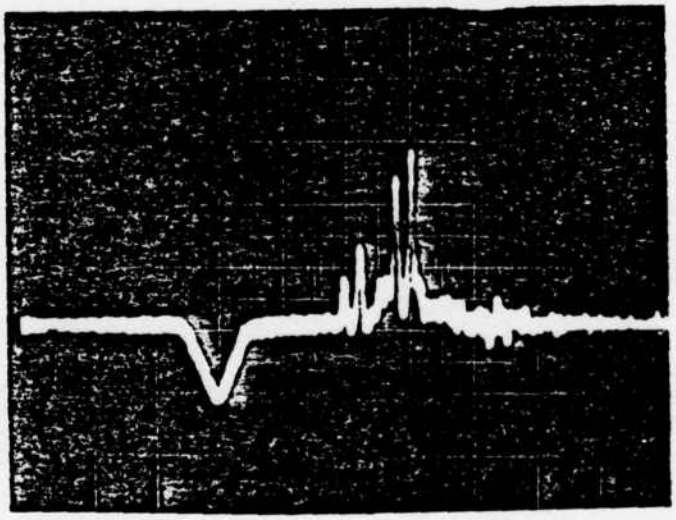

Figure 14. Typical R-band signal observed using 40 ns/div sweep speed on the oscilloscope. The negative signal is the time marker.

quency of the emission by the delay line technique.[28,29] This technique utilizes the fact that near the cut off frequency of a waveguide, f_c, the group velocity, v_g, of an electromagnetic pulse is frequency dependent and obeys the dispersion relation

$$v_g = c_g (1- f_c^2/f^2)^{1/2} \quad (7)$$

where c_g and f are the speed of light in the guide and the frequency of the pulse respectively. Thus for our experimental arrangement shown in Figure 15, the microwaves traveling down the 7.35 meter of waveguide will experience a frequency dependent delay, t, with respect to those detected by the 10cm length guide for the other detector. The delay and pulse frequency are related by

$$f = f_c (1-d^2/c^2t^2)^{1/2} \quad (8)$$

where d and c are the difference in lenghts of the two guides (7.25m) and the speed of light. f_c is 21.08 GH_z for the $TE_{1,0}$ mode.

Higher order modes either 1) will not propagate in the parallel plate transmission lines of the device and capacitor bank (TM), 2) will not be detected due to the placement of the antenna in the system detector ($TE_{m,n}$; m,n even), or 3) have a cutoff frequency higher than the maximum frequency to which the detector will respond ($TE_{3,0}$). Since the polarity of the emission is perpendicular to the parallel plates (see section B.2.1) and the $TE_{1,1}$ has a higher attenuation per unit length, the $TE_{1,0}$ is the mode detected by this method. The relationship between the delay time and frequency (Equation 8) is shown in Figure 16.

The delay line technique has been previously used to measure the emission spectra of microwaves generated in the propagation of relativistic electron

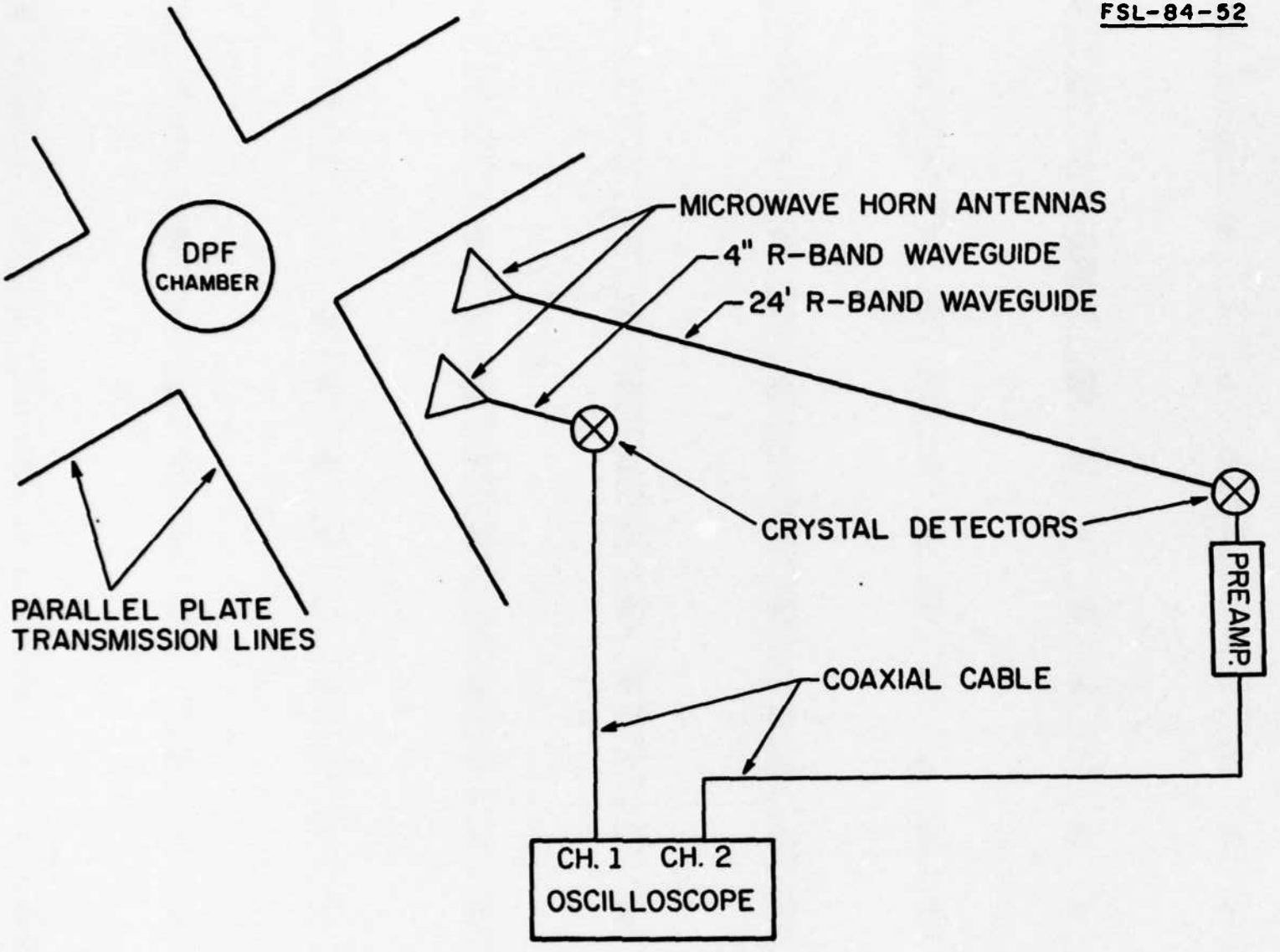

Figure 15. Schematic of the time of flight spectrometer.

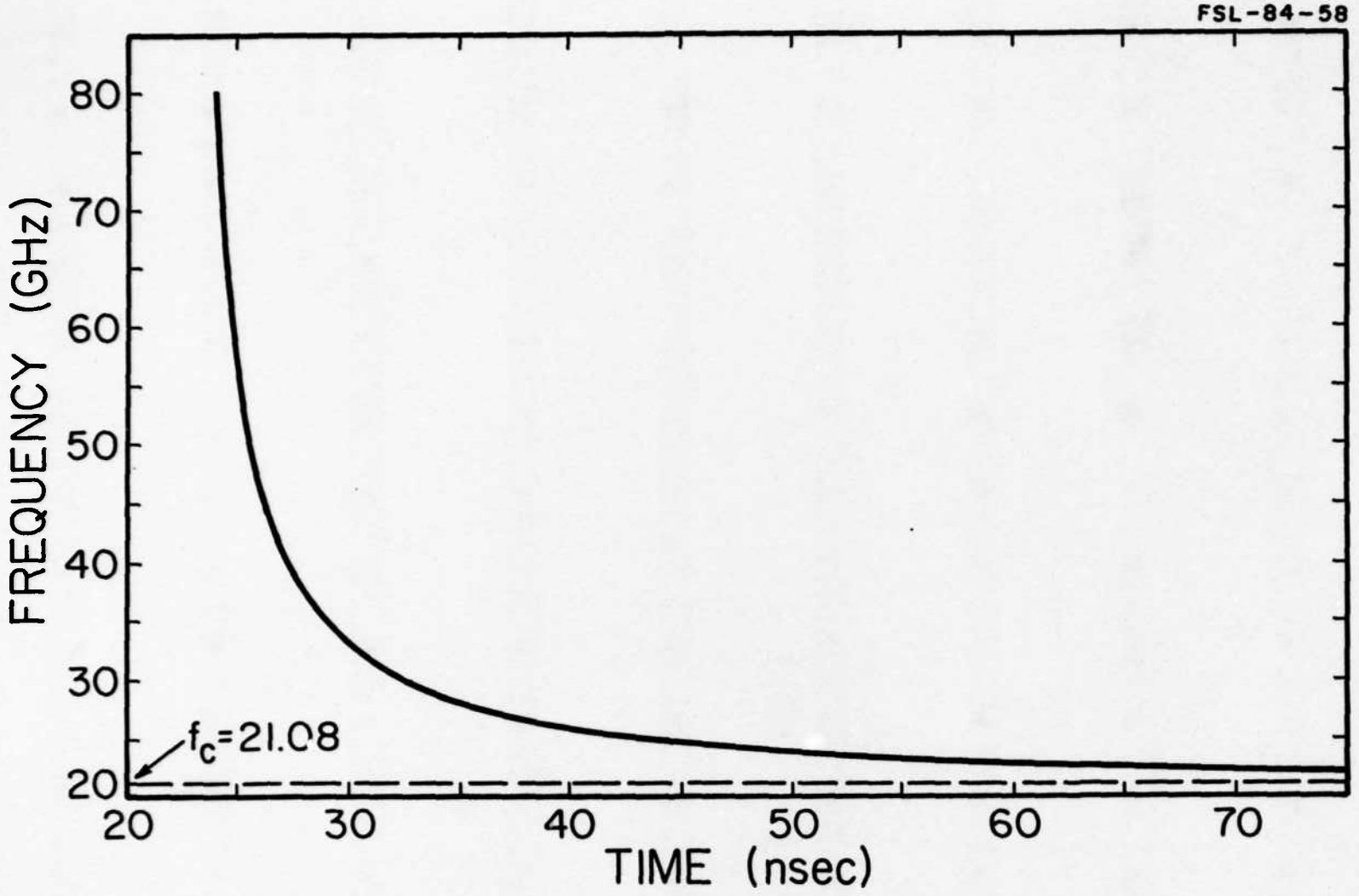

Figure 16. Transit time of a microwave pulse through 7.22 m of R-band (a=7.11 mm, b=3.56 mm) waveguide.

beams through gases[30] and to measure the output frequency of an electron synchrotron laser driven by an intense relativistic electron beam.[29] In addition, it was used to study the emission of microwaves[31] by the electron beam[5] generated by a plasma focus. These microwaves were emitted from a hole in the center electrode and were found to be high-power, narrowband millimeter waves ($P \sim 1MW$; $\Delta f/f < 5 \cdot 10^{-2}$; $30\ GHz < f < 120\ GHz$).

The origin of these latter microwaves is not the same as that of the microwaves studied here since a metal vacuum chamber below the center electrode prevented observation of electron beam generated microwaves and as will be demonstrated in the next section the period of emission of the microwaves does not coinside with the emission of the electron beams. Furthermore the current sheaths (Figure 12) are of sufficient density ($>10^{15}/cm^3$) and thickness (~1cm) to cutoff any millimeter waves from propagating from the region of the hole in the center electrode to the region between the inner and outer electrodes (Figure 12); no microwave radiation was detected coming from anywhere but from between the parallel plate of the capacitor bank.[27]

The experimental arrangement is shown in Figure 15. After a long experimental run twelve shots were found to have sufficiently few peaks in the R-band so that the delayed peak and its corresponding non-delayed peak could be identified. Two examples are shown in Figure 17. After corrections are made for varying cable lengths the frequency of the pulse may be determined.

From the twelve shots, fifteen frequencies could be determined. Two frequencies were found to be 28 GHz (±2GHz) and the rest lay between 23 and 24 GHz (±1GHz). Since these frequencies are close to cutoff (Figure 13) the accuracy of the measurement is quite good. All the data were taken with a capacitor bank energy of 12.5 kJ and a deuterium gas pressure between 3.0 and 3.6 torr.

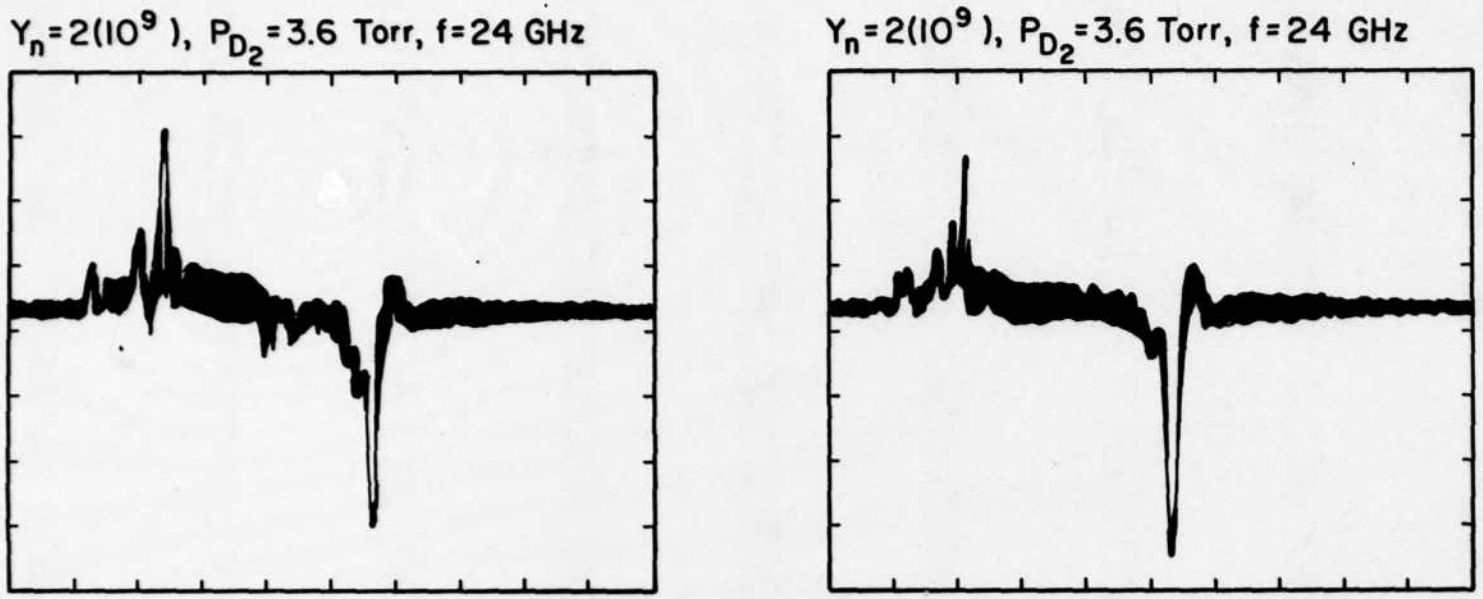

Figure 17. Time-of-flight spectrometer measurements.

Since it has been hypothesized that this emission is caused by current driven instabilities[21] it is of interest to compare these measurements with frequencies of the dominant modes of each of the current driven instabilities which may be candidates. These instabilities are:[23]

1) Buneman ($v_D > v_{the}$)
2) Ion Acoustic ($T_e >> T_i$)
3) Lower hybrid ($\beta < 1$)
4) Anisotropy-driven electromagnetic ($T_{i\perp} > T_{i\parallel}$)

where v_D, v_{the}, T_e, T_i, and β are the drift velocity of the electrons, their thermal velocity, their temperature, that of the ions, and the ratio of kinetic to magnetic pressure respectively. The plasma parameters for the plasma focus during the period of microwave emission are as follows:

Table II

Device Current, I	390kA
Plasma radius, r	0.39cm
Magnetic field at the plasma surface B_θ	20 Tesla
Plasma Temperature[11,32]	300 eV
Plasma density[33]	$5 \cdot 10^{18}/cm^{-3}$

The corresponding peak frequencies of the various current driven instabilities are shown in the following table:

Table III

Instability	Maximum Growth Rate Frequency[23]	Estimate of the Magnitude
Buneman	$1/2(m_e/2m_i)^{1/3} f_{pe}$	520 GHz
Ion Acoustic	$f_{pi}/\sqrt{3}$	192 GHz
Lower Hybrid	$9/4\ f_{LH} = 9/4\ (f_{ce}f_{ci})^{1/2}$	21 GHz
Anisotropy-driven electromagnetic	f_{ci}	0.15 GHz

where f_{pe}, f_{pi}, f_{ce}, f_{ci}, and f_{LH} are the electron and ion plasma, electron and ion-cyclotron and lower hybrid frequencies respectively.

The Buneman and anisotropy-driven electromagnetic instabilities have frequencies which differ the most from the measured value and hence probably can be eliminated from consideration as source candidates. The ion acoustic instability could act as a source in low density regions ($n_e < 7 \cdot 10^{16}/cm^3$) but the necessary condition for it to exist, $T_e \gg T_i$ is very unlikely to occur in a shock heated plasma.[34]

Hence the most likely candidate is the lower hybrid instability which occurs in regions of strong magnetic field gradients and hence the value quoted in the table is really an upper limit to its magnitude.

B.2.3 Time sequence of the microwave emission with various phenomena that characterize a plasma focus discharge.

In order to test possible physical models the time of the microwave emission was compared with several other phenomenon associated with the discharge. These other phenomenon were:

Phenomenon	Diagnostic
1) Time derivative of the device current	Rogowski coil

2) Soft Xray emission	Pindiode detectors and various filters
3) Current sheath dynamics	Radial and axial streak pictures
4) Hard Xray and neutron emission	Fast scintillator and PM tube
5) Electron beam emission in various energy bands	Magnetic Spectometer

The magnetic spectrometer was attached to the bottom of the anode so it could sample the electron beam passing down the hole in the center electrode as shown in Figure 18. The ranges of energy sampled by a given channel of the spectrometer are given in Figure 19. Also shown in Figure 18 is the location of the Rogowski coil to which was used to measure the time derivative of the device (or main bank) current. The arrangement to measure the soft Xray emission is shown in Figure 20; the long collimating tube betweeen the pindiodes and the DPF chamber restricts the observed region of the pinch to a spot on the device axis 2mm in diameter and 5mm above the center electrode. The photomultiplier tube and scintillator were placed 3.96m away from the position of the pinch and the tube has inherent delay of 40 ±7ns. Corrections for time-of-flight and cable delays have been made in the data reported below. No external magnetic field was applied to the discharge during the experiments reported here.

The results for the various phenomena excluding the streak picture are shown in Figure 21 and typical comparisons between signals are shown in Figures 22-24. The two soft Xray pulses are due to two densifications along the device axis: the first being the initial compression of the plasma column and the second several seperate densifications along the axis. The latter signals the breakup of the pinch and is probably caused by mhd instabilities(Figure 5).

These results show that the electron beam and the microwaves are not directly

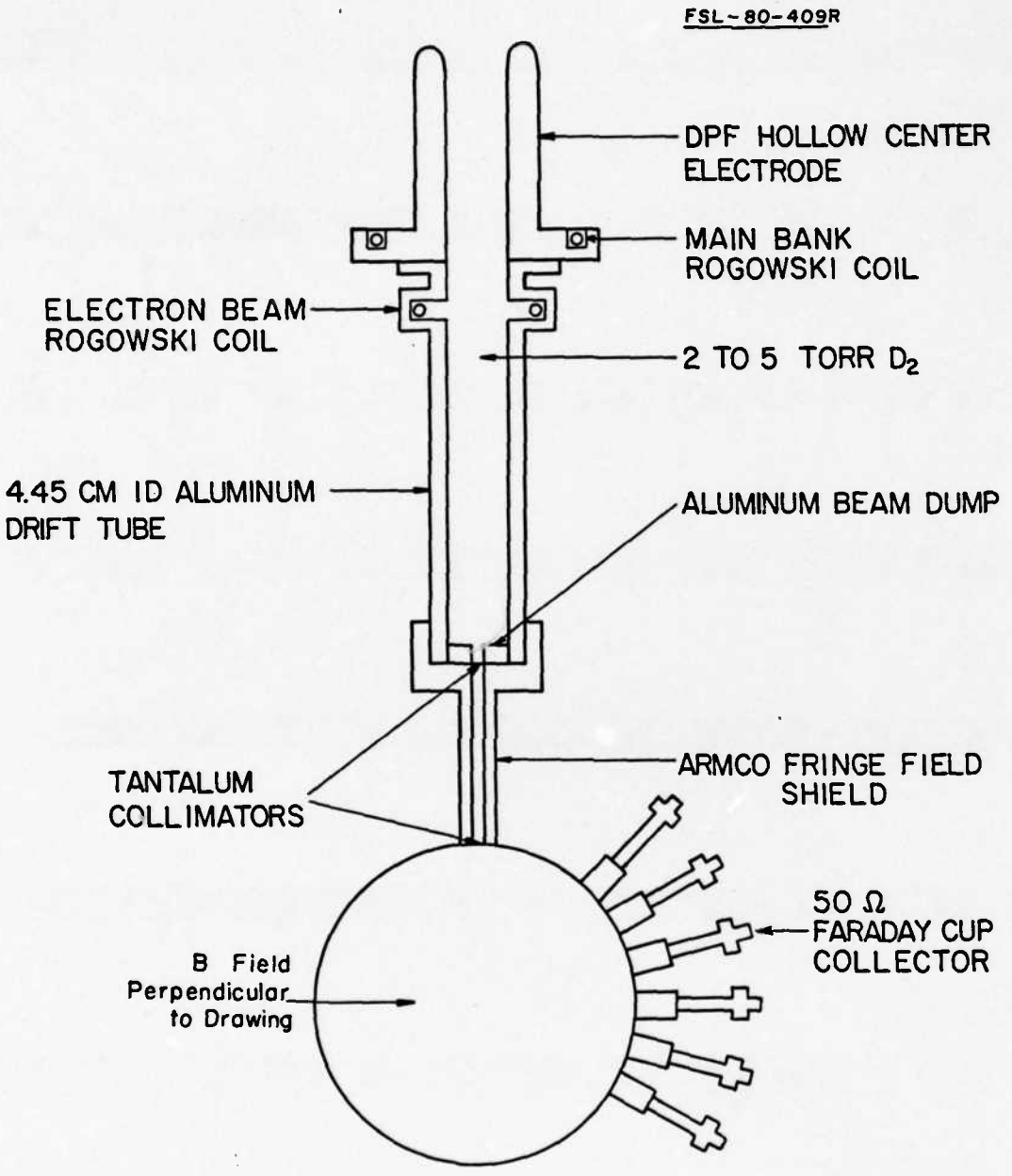

Figure 18. Electron Beam Spectrometer.

Figure 19. Electron Beam Spectrometer Energy Channels

Spectrometer Channel	Lower Energy Limit (keV)	Nominal Center Energy (keV)	Upper Energy Limit (keV)
45°	19	25	34
60°	38	49	61
75°	68	83	101
90°	111	133	160
105°	176	184	252
120°	277	333	404

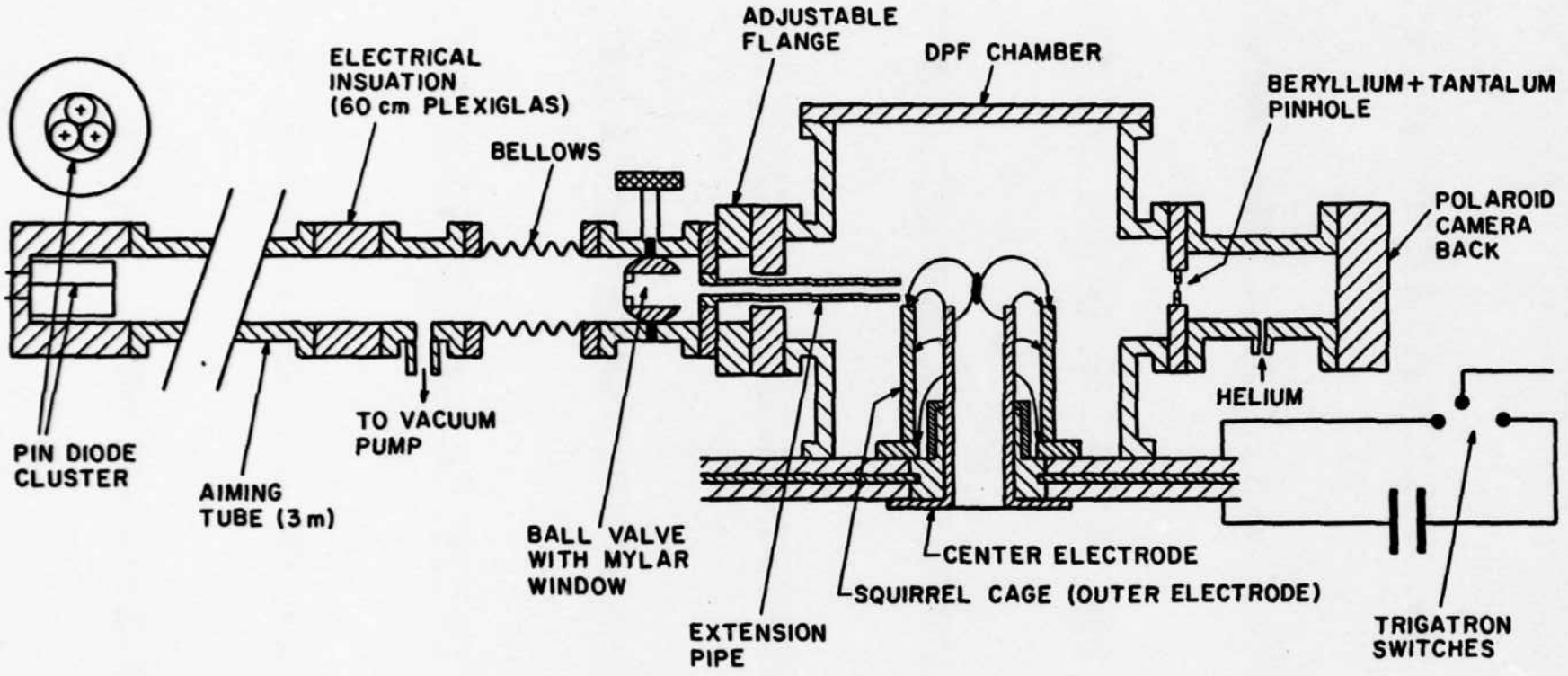

Figure 20. Experimental arrangement to detect soft x-rays.

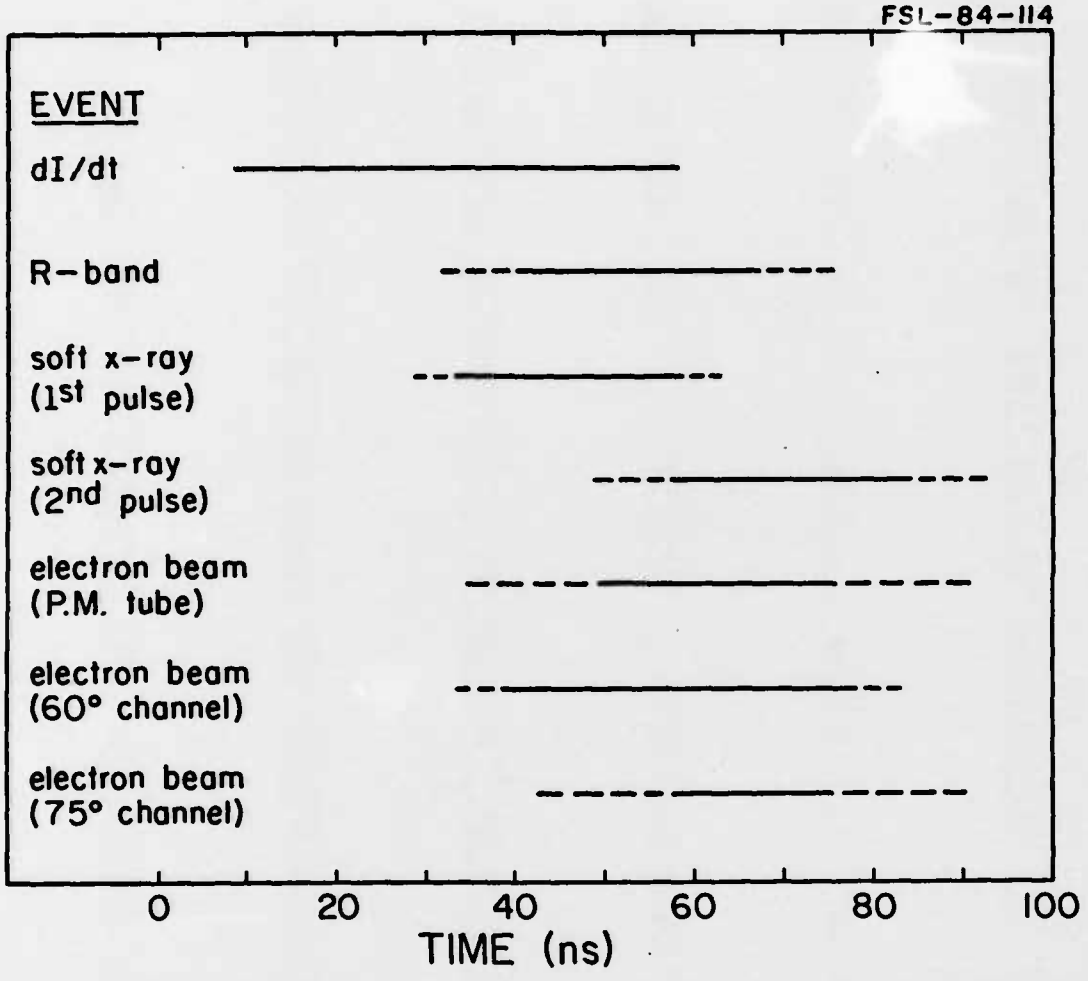

Table 21. Temporal comparisons of various events occurring in the plasma focus during the time of the pinch. The mean time at which the peak in the signal occurs is at the center of each line. The solid represents the average duration at full width at half the maximum (FWHM) of the signal. The broken line represents the statistical variation with respect to dI/dt.

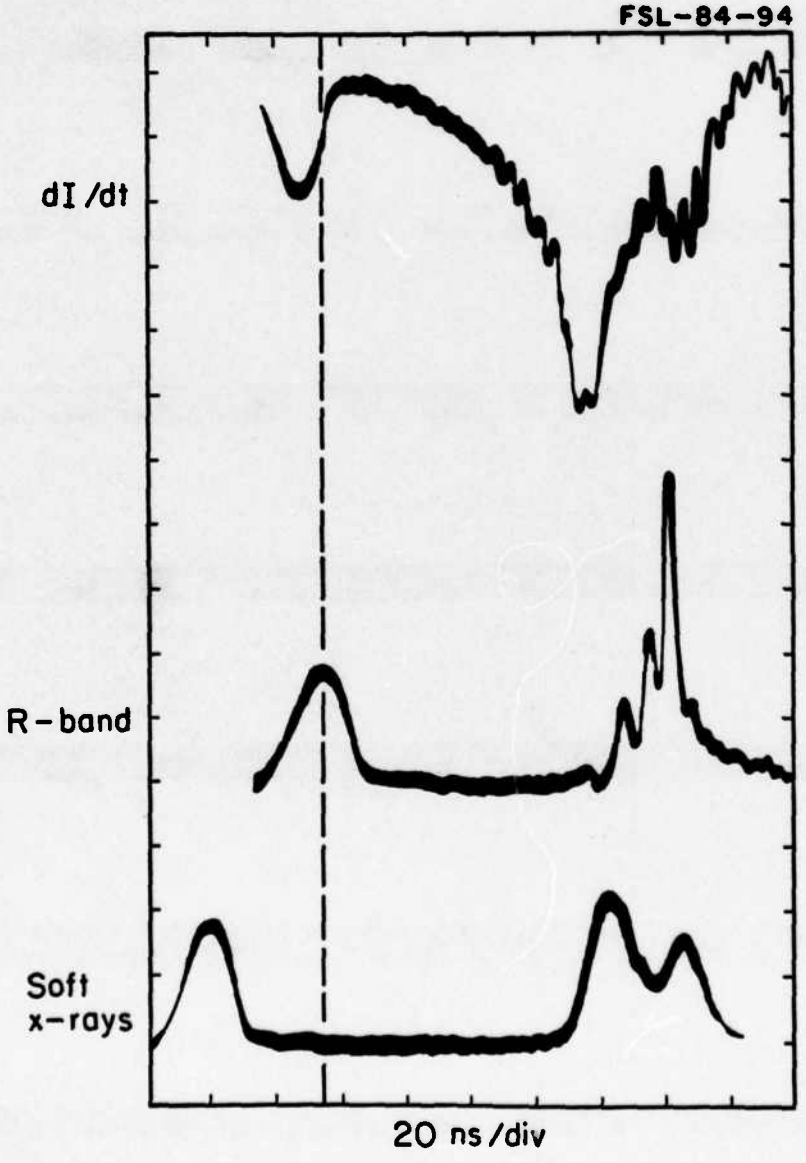

Figure 22. Simultaneous waveforms comparing the time of the R band emission with respect to the current interruption ($\dot{I}$) and the soft x-ray emission. The initial peaks are simultaneous time markers whose positions have been adjusted to reflect differences in cable lengths and time-of-flight.

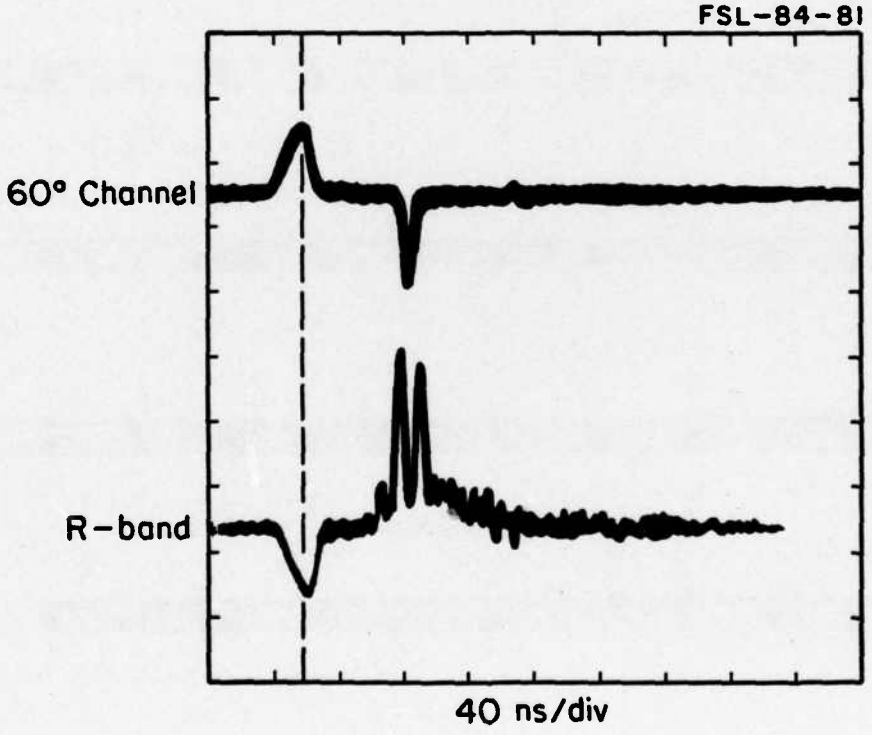

Figure 23. Simultaneous waveforms comparing the occurrence of the emission of the R band and the 49 keV portion of the electron beam (60° channel on the electron spectrometer, Figures 18 and 19). The initial peaks on the waveforms are simultaneous time markers whose positions have been adjusted to reflect differences in cable lengths and times-of-flight.

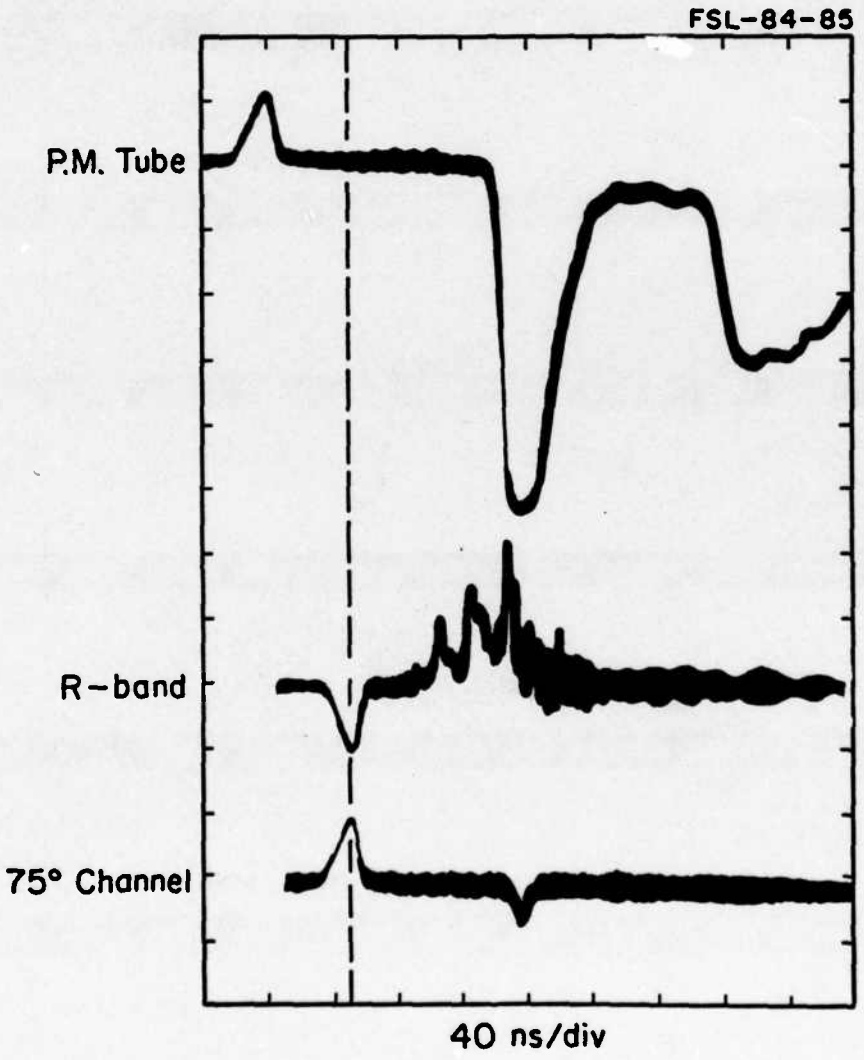

Figure 24. Simultaneous waveforms comparing the occurrence of the emission of the R band, the 83 keV portion of the electron beam (75° channel on the electron spectrometer, Figures 18 and 19) and the hard x rays (P.M. tube). The initial peaks on the waveforms are simultaneous time markers whose positions have adjusted to reflect differences in cable lengths and times-of-flight. The last peak on the PM tube signal is due to 2.45-MeV neutrons generated by $D(d,n)^3He$ reactions in the device. The position of this peak has not been adjusted for time-of-flight.

related since they do not occur at the same time. This correlation might have been expected given the results from other DPF devices.[31]

B.2.4 Preliminary Model

These results have been used to formulate a model for the microwave emission and enhanced resistivity that is being tested at present.

The essence of the model is that the microwaves and enhanced resistance are caused by current driven instabilities occuring in the thin current sheath (5 plasma skin depths thick) produced on the outer boundary of the pinch during 1st compression. This is similar to the model developed by Peacock and his co-workers[35] to explain the results of their laser scattering and Faraday rotation experiments.[36] Their results indicate that at the maximum in the 1st compression the current sheath is confined to a thin outer skin. The current flow redistributes itself in the next tens of nanoseconds permitting 30% of the current to flow in the interior. Blue shifts of the scattered light indicate that the local electron drift velocity in the outer skin ranges between one to one-tenth times their thermal speed. Enhanced scattering from this region indicates the presence of ion turbulence.[37]

This model for the experimental results from Culham is further supported by laser scattering results from Frascati on their last 1MJ DPF facility. The larger diameter plasma produced by that device (diameter of 1.4 cm versus 0.5 cm for the Culham device) permitted the Frascati scientists to scatter laser light from distinct regions to the plasma. They found enhanced scattering from the outer regions and thermal scattering from the core during the period between maximum compressions and the onset of neutron production.[38] The presence of a turbulent outer skin current following first compression is therefore fairly well established experimentally.

Applying the model to our results the following predictions will be compared with experiment:

1. Frequency of the microwave emission
2. Resistance of the pinch versus time
3. Duration of the microwave burst
4. The timing of the burst
5. The power level of the burst

The results of these comparisons will be reported next fall in the Annual Report for another grant (Grant No. AFOSR-84-0391).

References for Final Report

1. J. Mandrekas, F. Venneri, and G. Gerdin, 1982 IEEE Int. Conf. on Plasma Sci., IEEE No. 83CH1770-7, 117 (1982).

2. G. Gerdin, W. Stygar, F. Venneri, J. Appl. Phys 52, 3269 (1981).

3. G. Gerdin, J. Durham, and R. Ilic, Nuclear Tracks, 5, 299 (1981).

4. G. Gerdin, W. Stygar, and F. Venneri, Bult. Amer. Phys. Soc., 26, 849 (1981).

5. W. Stygar, G. Gerdin, F. Venneri and J. Mandrekas, Nucl. Fusion, 22, 1161 (1982).

6. M. J. Rhee, B. S. Park, and R. F. Schneider, Bult. Amer. Phys. Soc., 29, 1282 (1984).

7. L. Pokora, "Unconventional Methods and Sources of Laser Pumping," Proc. of Symposium Optics '84, April 24-27th, 1984 Budapest, Hungary.

8. J. Salge, "Problems of Repititive Opening Switches Demonstrated on Repetive Operation of a Dense Plasma Focus," Workshop on Repetitive Opening Switches, M. Kristansen and K. H. Schoenbach ed., Texas Tech. University, Lubbock, TX 79409, 189 (1981).

9. J. Salge, U. Braunsberger, B. Fell, I. Ueno and H. Conrads, Nucl. Fusion, 18, 972 (1978).

10. L. Spitzer, Physics of Fully Ionized Gases, 2nd ed., (Interscience, 1962) 108.

11. G. Gerdin and F. Venneri, Bult. Amer. Phys. Soc., 27, 1064 (1982).

12. J. W. Mather, Methods of Experimental Physics 9B (Academic Press, 1971) 187.

13. T. F. Stratton, in Plasma Diagnostic Techniques (R. H. Huddleston, S. L. Lenard, eds, Academic Press, 1965) 201.

14. C. DeMichelis, M. Mattioli, Nuclear Fusion, 21, 677 (1981).

15. D. J. Johnson, Rev. Sci. Instrum. 45, 191 (1974).

16. P. G. Eltgroth, Phys. Fluids, 25, 2408 (1982).

17. Y. Kondoh and K. Hirano, Phys. Fluids, 21, 1617 (1978).

18. F. Venneri, J. Mandrekas, and G. Gerdin, Proc. of the 4th IEEE Int. Pulsed Power Conf. Albuquerque, NM, pg. 350-53 (June 6-8, 1983).

19. F. Venneri, H. Krompholz, J. Mandrekas, G. Gerdin, and M. Tanis, Bult. Amer. Phys. Soc., 28, 1171 (1983).

20. O. A. Anderson, W. R. Baker, S. A. Colgate, J. Ise Jr, and R. V. Pyle, Phys. Rev., 110, 1375 (1958).

21. K. Schonbach, H. Krompholz, L. Michel and G. Herziger Phys. Lett. 62A, 430 (1977), and G. Herziger, H. Kromphoz, L. Michel and K. Schonbach Phys. Lett. 64A, 51, (1977).

22. G. Bekefi, Radiation Processes in Plasma (John Wiley and Sons, 1966) 141.

23. R. C. Davidson and N. A. Krall, Nuclear Fusion, 17, 1313 (1977).

24. J. Mandrekas, M.S. thesis, University of Illinois (1984).

25. F. F. Chen, "Electric Probes," in R. H. Huddlestone and S. L. Leonard Ed., Plasma Diagnostic Techniques (Academic Press, 1965) 113.

26. W. H. Bostick, V. Nardi, W. Prior, Bult. Amer. Phys. Soc., 18, 1364 (1973).

27. M. Tanis, M.S. thesis, University of Illinois (1984).

28. J. A. Nation, Rev. Sci. Instrum., 41, 1097 (1970).

29. V. L. Granastein, P. Sprangel, R. K. Parker, and M. Herdon, J. Appl. Phys., 46, 2021 (1975).

30. J. A. Nation and W. L. Gardner, Nuclear Fusion, 11, 5 (1971).

31. K. Schmitt, H. Krompholz, F. Ruhl and G. Herziger, Phys. Lett., 95A, 239 (1983).

32. F. Venneri, G. Gerdin, 1984 IEEE Int. Conf. on Plasma Sci., Conf Record-Absract, IEEE Catalog No. 84CH1958-8, 107 (1984).

33. A. Bernard, A. Coudeville, A. Jolas, J. Launspach and J. DeMascureau, Phys. Fluids, 18, 180 (1975). These measurements were on a plasma focus device with the same peak current (600kA) and the same electrode dimensions as our device. These similarities plus the fact that pinch density does not change significantly between DPF devices of greatly varying input energy lend support to using this number. For example the 250kJ DPF device at Frascati has the same density range $5 \leftrightarrow 8 \cdot 10^{18}/cm^3$ as the 27kJ device referenced above. See J. P. Rager et al, in Plasma Phys. and Controlled Nucl. Fusion Res., (Proc. 9th Int. Conf. Baltimore, 1982) IAEA Vienna (1982).

34. E. Fermi, Phys. Rev., 75, 1169 (1949).

35. R. E. Kirk, M. J. Forrest, D. G. Muir, and N. J. Peacock, Proc. of the 3rd Int. Workshop on Plasma Focus Res., H. Herold and H. J. Kaeppeler eds., Plasma Res. Institute, Univ. of Stuttgart Rep. (IPF-83-6), 119 (Sept. 1983).

36. D. G. Muir, PhD. Thesis, Univ. of London (1983).

37. N. J. Peacock, R. J. Speer, and M. G. Hobby, J. Phys. B Ser. 2, 2, 798, (1969).

38. J. Ehrhardt, P. Kirchesch, K. Huebner and J. P. Rager, Phys. Letts., 89A, 285, (1982).

C. Cumulative Chronological List of Publications

1. G. A. Gerdin, W. Stygar, and F. Venneri, "Faraday Cup Analysis of Ion Beams Produced by a Dense Plasma Focus," J. Applied Physics, 52, 3269-3275 (1981).

2. G. A. Gerdin, J. Durham, and R. Ilić, "Solid State Nuclear Track Detectors and High Fluences of Light ions," Nuclear Tracks, 5, 299-309 (1981).

3. W. Stygar and G. A. Gerdin, "High Frequency Rogowski Coil Responce Characteristics," IEEE Trans. on Plasma Science, Vol. PS-10, pp 40-44 (1982).

4. W. Stygar, G. Gerdin, F. Venneri, J. Mandrekas., "Particle Beams Generated by a 6-12•5 kJ Dense Plasma Focus," Nuclear Fusion, 22, pp. 1161-72 (1982).

5. G. Gerdin, Book Review of Plasma Physics (Vol. 8) M. A. Lenontovich, Ed., Plenum (1980) Nuclear Technology, 58, pp. 551-53, 1982.

6. F. Venneri, J. Mandrekas, and G. Gerdin, "Preliminary Studies of the Plasma Focus as an Opening Switch," Proc. of the 4th IEEE Inter. Pulsed Power Conf. Albuquerque, NM, pp. 350-353 (June 6-8, 1983).

7. M. Tanis, G. Gerdin, F. Venneri, "Microwave Emission and Enhanced Resistance in a Dense Plasma Focus," in preparation.

D. List of Professional Personnel Associated with the Research Effort Personnel

Personnel

Glenn Gerdin, Asst. Professor, Nuclear Engineering, Principal Investigator

William Stygar, graduate assistant supported by AFOSR (supported until end of Fall Semester of 1981)

James Durham, graduate assistant supported by U. of I. Research Board, June 1980-Aug. 1981

Francesco Venneri, graduate assistant supported by AFOSR, Jan. 1980 to present

John Mandrekas, graduate assistant supported by AFOSR Fall 1982-Dec. 1983

Mark Tanis, graduate assistant supported by AFOSR June 1983-July 1984

Kevin Boulais, graduate assistant supported by AFOSR Sept. 1984-present

Advanced Degrees

Jan. 1980, William Stygar, Master of Science in Nuclear Engineering, University of Illinois at Urbana-Champaign, thesis title: "Design, Construction, and Operation of a fast Rise Time, High Voltage Pulse Generator."

Jan. 1982, William Stygar, Doctor of Philosophy in Nuclear Engineering, University of Illinois at Urbana-Champaign, thesis title: "An Experimental and Theoretical Investigation of Electron Beams Generated by a Dense Plasma Focus."

Jan. 1984, James Durham, Master of Science in Nuclear Engineering, University of Illinois at Urbana-Champaign, thesis title: "Use of Solid State Nuclear Track Detectors as a Diagnostic for a Dense Plasma Focus."

April, 1984, John Mandrekas, Master of Science in Nuclear Engineering, University of Illinois at Urbana-Champaign, thesis title: "Zero-Dimensional Model for the Dense Plasma Focus."

July, 1984, Mark Joray Tanis, Master of Science in Nuclear Engineering, University of Illinois at Urbana-Champaign, thesis title: "Microwave Emission from a Dense Plasma Focus.

F. Interactions

Conference Papers

1. Stygar, W. and Gerdin, G. A., "Phenomena Associated with Particle Beam Generation in a Plasma Focus," Bull. APS, 24, No. 8, Oct. 1979, p. 1039.

2. Gerdin, G. A., Stygar, W., and Venneri, F., "Ion and Electron Current Measurements in a Plasma Focus Device." IEEE International Conf. on Plasma Science, Conf. Record, Madison, Wisc. May 1980. P. 75.

3. Stygar, W., Gerdin, G. A., Venneri, F., "Simultaneous Electron and Ion Beam Measurements in a Plasma Focus," Bull. APS, 25, No. 9, October 1980.

4. Ilic, R., Gerdin, G., Durham, J., Wehring, B., Stygar, W., Emoto, T., "Dense Plasma Focus Studies with Solid State Nuclear Track Detectors (SSNTD).", Bull. APS, 25, No. 9, October 1980.

5. Stygar, W., Gerdin, G., Venneri, F., Durham, J., and Mandrekas, J., "Characteristics of Electron beams Generated by A Dense Plasma Focus," IEEE International Conference on Plasma Science, Conference Record, Santa Fe., NM., May 1981, P. 121.

6. Gerdin, G. Stygar, W., and Venneri, F., "Plasma-Focus Electron-Beam Scaling Experiments," Bull. APS, 26, No. 7, Sept. 1981, p. 849.

7. Mandrekas, J., Venneri, F., and Gerdin, G., "Beam Particle Measurements and Neutron Production in a 6-12 kJ Plasma Focus." IEEE Inter. Conf. on Plasma Science, Conf. Record Abstracts, Ottawa, Canada, May 1981, P. 117.

8. Stygar, W., Mandrekas, J., Gerdin, G., "1-D Computer Modeling of a Plasma Focus Including Anomalous Transport," Bull. APS 27, p. 1063, 1982.

9. Gerdin, G. and Venneri, F., "Operation of a Plasma Focus Using Gas Mixtures," Bull. APS, 27, p. 1064, 1982.

10. Venneri, F. and Gerdin, G. "Preliminary Studies of the Plasma Focus as an Opening Switch," IEEE Inter. Conf. on Plasma Science, Conf. Record, San Diego, CA. May 1983, pp. 59-60.

11. Venneri, F., Krompholz, H., Mandrekas, J., Gerdin, G., Tanis, M., "Preliminary Results of the Plasma Focus as an Opening Switch," Bult. APS, 28, pp. 1171 (1983).

12. Tanis, M., Gerdin, G., "Microwave Emission from the Dense Plasma Focus," IEEE International Conf. on Plasma Science, Conf. Record Abstracts, St. Louis, MO., May 1984, P. 104.

13. Venneri, F. and Gerdin, G.,"Dense Plasma Focus as an Opening Switch," IEEE International Conf. on Plasma Science, Conf. Record Abstracts, St. Louis, MO, May 1984, p. 104-105.

14. Venneri, F. and Gerdin, G., "Soft x-ray Analysis of a Dense Plasma Focus" IEEE International Conf. on Plasma Science, Conf. Record Abstracts, St. Louis, MO, May 1984, p. 107.

15. Gerdin, G. A., and Venneri, F., "Sequence of Phenomea Occuring During the Pinch Phase of a Dense Plasma Focus," Bull. APS, 29, p. 1266, (Oct. 1984).

Collaboration

May 1980 to Aug. 1980, Radomir Ilic, University of Ljubljana, Ljubljana, Yugoslavia on solid state nuclear tract detectors as diagnostic tools for Fusion experiments.

Jan. 1982 - present, Professors K. H. Schoenbach, H. Krompholz, K. Kristinasen of Texas Tech University on Opening Switch Research.

PARTICLE BEAMS GENERATED BY A 6–12.5 kJ DENSE PLASMA FOCUS†

W. STYGAR*, G. GERDIN, F. VENNERI,
J. MANDREKAS
Fusion Studies Laboratory,
214 Nuclear Engineering Lab.,
Urbana, Illinois,
United States of America

ABSTRACT. Particle beam diagnostic tools involving an ion beam Faraday cup, an electron beam Faraday cup, an electron magnetic spectrometer and solid-state nuclear track detectors have been used to measure the parameters of the particle beams generated by a Mather-type dense plasma focus. At a capacitor bank energy of 12.5 kJ, the energy spectra of the electron and ion beams are found to obey the same power laws: $dN/dE \propto E^{-x}$ where $x \cong 3.5 \pm 0.5$. Primary electron beam current and energy spectra were measured as a function of main bank current at pinch time, I_{MB}. The primary electron beam current was found to scale as $I_{MB}^{2.9\pm0.5}$, reaching a magnitude of 17 kA for a device energy of 12.5 kJ. The exponent x of the electron energy spectra was found to scale as $x \propto I_{MB}^{1.15\pm0.2}$. These results are incorporated into an axial beam target model for neutron production, and it is found that this model could account for the magnitude and scaling of the observed neutron yield with I_{MB}.

1. INTRODUCTION

The measurement of the energy spectra of particles accelerated by a plasma focus (Fig. 1) is of interest for several reasons. One is to clarify the mechanism of neutron production by using the measured ion energy spectra to predict the beam-target component of the neutron yield. A second reason is to further define the acceleration process by comparing the direction and energy spectra of the various particle species emitted. The definition of the acceleration process would make possible scaling predictions for the use of the dense plasma focus (DPF) as an accelerator and/or as an inertial confinement fusion driver. Also electrical energy appears to be coupled to the plasma focus by current interruption [1] and since current interruption has been proposed as mechanism for particle acceleration in solar flares [2], the results of such studies may have applications to astrophysics as well.

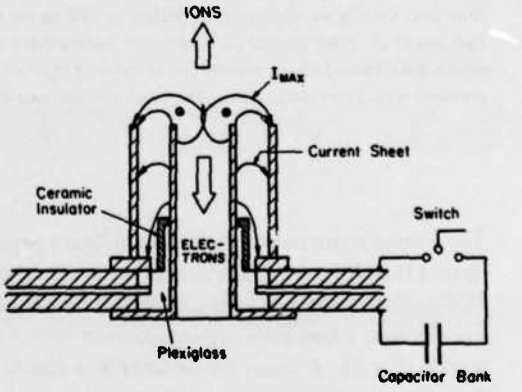

FIG. 1. Plasma focus device. During current interruption at pinch time the ions and electrons are accelerated in directions shown.

Figure 2 illustrates that current interruption is a source of energy in a plasma focus. The lowest trace is the main bank current waveform of the plasma focus. The sharp reduction in the current by a factor of two at pinch time indicates [1] that one-half the magnetic energy was coupled into the pinch (i.e. 3.8 kJ).

† This article is based on a portion of the PhD thesis submitted by one of the authors (WS) in partial fulfilment of the requirements for the doctoral degree at the University of Illinois.

* Present address: Sandia National Laboratory, Albuquerque, New Mexico, 87185, USA.

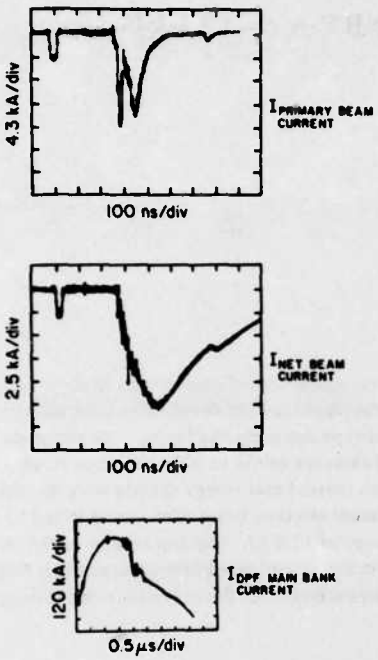

FIG.2. Simultaneous waveforms of fast electron primary current as measured on fast Faraday cup (top), net electron current signal as measured on Rogowski coil mounted on electron drift tube (middle; see Fig.4) and current flowing in the DPF as measured by a Rogowski coil mounted on anode (bottom, see Fig.4). Rectangular pulses at 100 ns on the top two traces are time markers and electron currents are simultaneous with end of dip in plasma focus current (±50 ns). Filling pressure was 3 torr deuterium; the bank voltage was 25 kV.

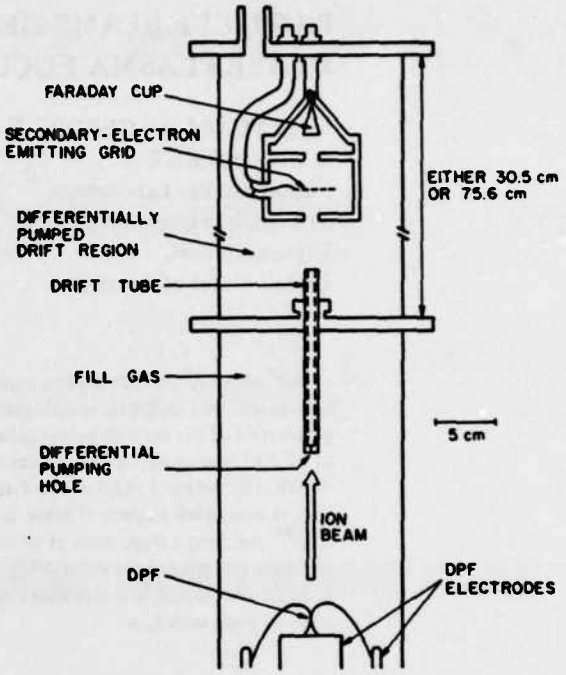

FIG.3. Ion Faraday cup time-of-flight arrangement. Differential pumping hole is 0.48 cm long.

The primary current of the electron beam generated during the DPF current interruption is also shown in Fig.2. This is the signal of a slightly modified Pellinen [3] electron beam Faraday cup located below the device (Fig.1). A 6-μm mylar filter was placed over the cup to permit the observation of the primary electron beam current. The time markers show that the fast electrons are generated during the sharp drop in the focus current, indicating that current interruption is converting a fraction of the magnetic energy to particle kinetic energy.

In this paper, the first simultaneously observed energy spectra of ions and electrons emitted from a plasma focus are reported. Also the scaling of the primary electron beam current and energy spectrum with the total DPF main bank current at pinch time, I_{MB}, are reported for the first time [4]. The ions and electrons are accelerated in the directions shown in Fig.1. The ion beam energy spectra were measured with a Faraday

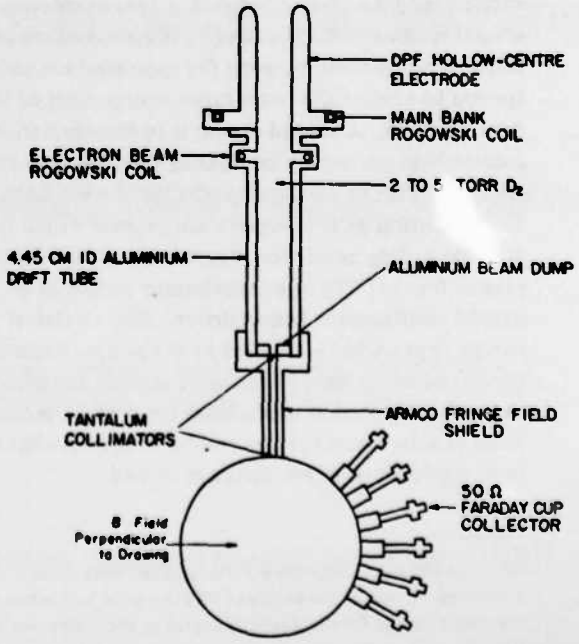

FIG.4. Schematic view of electron magnetic spectrometer.

cup and time-of-flight analysis [5] (Fig.3) and the electron beam energy spectra with a magnetic spectrometer (Fig.4).

Previous measurements of the DPF ion beam energy spectra have been made with activation analysis [6–8], magnetic spectrometers [9, 10], time-of-flight analysis with doubly diffused Si (PIN) detectors [11, 12], Thomson spectrometers [13, 14], and nuclear emulsions [15]. However, the time-of-flight arrangement used in this work can resolve the ion energy spectrum down to lower energies [5] than any of the other methods, which is significant since the electron beam energy spectrum will be shown to have a large component in this lower energy range.

The electron beam energy spectrum of the plasma focus has generally been inferred by analysis of the hard X-ray emission spectrum [16–21] or of dendrite patterns [21–23] caused when the fast electrons strike a target such as plexiglas. The hard-X-ray emission energy spectra are observed [16–19, 21] to have a power law dependence decreasing with photon energy, but it is not possible to uniquely determine the electron energy spectra from such X-ray measurements. Usually, a thick-target bremsstrahlung model and a power-law electron energy spectrum are assumed in order to evaluate the exponent of the power law [16]. Analysis of dendrite patterns in target materials is cumbersome and the lower limit of the observable energy is about 100 keV [22].

The magnetic spectrometer used in this work has none of these drawbacks and while this type of spectrometer has been used to study electron beams generated by vacuum diodes [24, 25], this is the first time it has been used to study the fast electrons emitted by a plasma focus.

In the next four sections, the apparatus and the results are presented and discussed and conclusions relating to neutron production and the acceleration process are drawn.

2. THE EXPERIMENTAL APPARATUS

The Illinois DPF has Mather-type electrodes as shown in Fig.1. The centre electrode (anode) is hollow to permit direct observation of fast particles emitted from the lower end of the pinch. The outer diameter of the centre electrode is 5.08 cm and the inner diameter of the squirrel cage (outer electrode) is 10.2 cm. The centre electrode extends 14 cm beyond a lavite insulator [26]. The electrode material is OFHC copper; there is evidence that oxygen released from regular copper during a discharge is detrimental to focus formation [27]. The DPF capacitor bank (40 μF, 60 kV) is composed of four modules, each of which is switched by a trigatron spark gap. A trigger pulse generator has been built [28] which provides 80 kV pulses with a 10–90% rise-time of less than 5 ns to trigger the switches. The jitter in the switch closure time is measured to be less than 4 ns. The capacitor bank modules are coupled to the DPF electrodes via four low-inductance parallel-plate transmission lines arranged symmetrically around the focus. The total circuit inductance external to the DPF electrodes is 17 nH. The DPF chamber is pumped down to 1 μm between shots by a trapped two-stage roughing pump.

For the measurements reported here the bank voltage was 16 to 25 kV, the deuterium fill gas pressure was 3 torr and the bank current at pinch time was up to 560 kA. Under these conditions the average neutron yield is 3.8×10^9 and the peak yield is 7.5×10^9. At constant pressure (3 torr deuterium), the neutron yield is found to scale as the plasma focus current at pinch time to the power of 4.4 (Fig.5). The bank voltage was limited to 25 kV and below for the results reported here. This limit was selected because flashover damage to the capacitor bank insulation occurred at this voltage when the device was operated at a fill pressure of 1 torr D_2. The device was normally operated at a higher pressure (3 torr) which is predicted

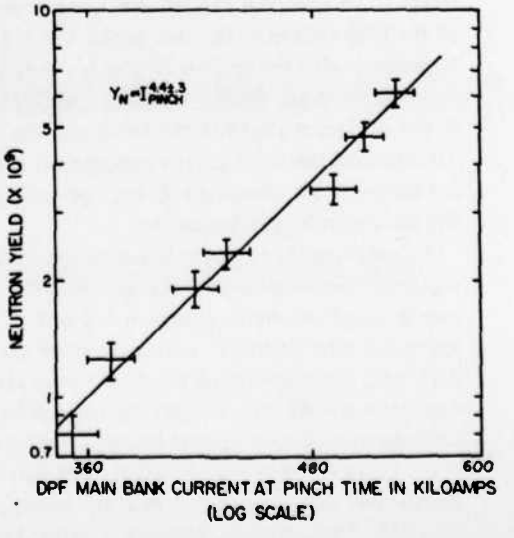

FIG.5. Plot of neutron yield versus plasma focus current at pinch time. Filling pressure was 3 torr deuterium; bank voltage range 16–24 kV.

[29] to lower the induced voltage across the device and hence provide some margin of safety.

The energy spectra of the ions and electrons reported here are those of particles directed along the symmetry axis of the device and in the direction of the current flow for each species. Since the outer electrode is negative with respect to the centre electrode the ions move away from the centre electrode and the electrons pass through it (Fig.1). The ion energy spectrum was measured with a magnetized Faraday cup and time-of-flight analysis; details are reported elsewhere [5]. The basic feature of the time-of-flight arrangement is the use of a re-entrant drift tube with a 0.046-cm-diameter hole on the end placed 16 cm above the anode on the device axis (Fig.3). Most of the 48 cm ion flight path is differentially pumped to 15 μm and thus the effects of energy attenuation and multiple scattering of the ions by the gas molecules are greatly reduced, allowing resolution of the ion energy spectra down to 25 keV.

The instant of acceleration for time-of-flight analysis is taken to be the onset of the hard X-rays observed with a plastic scintillator-photomultiplier tube combination. It is assumed that the electrons accelerate at the same instant as the ions and produce thick-target bremsstrahlung when striking the centre electrode or the vacuum chamber. Although the analysis assumes that only one ion species (i.e. D^+) is present, this assumption is consistent with the observation that with deuterium gas only one peak in the Faraday cup signal is observed [5] and nearly equal amounts of hydrogen and deuterium must be present for two peaks to be observed [5]. In the latter case, the ratio of the flight times of the two peaks is ~ 1.4 which is consistent with the species H^+ and D^+ undergoing ion diode acceleration [30] followed by multiple scattering in the gas target ahead of the beam (see Section 4). To interpret the ion Faraday cup signals, corrections are made [5] for charge state, multiple scattering by the gas and energy attenuation.

To measure the electron beam energy spectrum, the electron beam is transported from the DPF to the magnetic spectrometer as shown in Fig.4. The drift space diameter of the 25 cm long hollow anode is 3.18 cm; the diameter of the 45 cm long aluminium drift tube is 4.45 cm. Similar dimensions have been used previously to transport electron beams (with $\nu/\gamma \ll 1$ and $\nu/\gamma \approx 1$) with less than 20% loss of beam charge over distances of ~ 1 m at optimum pressure [31, 32]. The optimum pressure is defined to be that pressure at which the electron beam charge is transported with minimum loss [33, 34], and is also the pressure at which a beam is transported with the least amount of change in its energy spectrum [35]. For deuterium, the optimum pressure range (80% transmission) for beams with $\nu/\gamma \approx 1$ is from 2 to 5 torr [33, 34]; consequently, the same gas used in the DPF chamber (i.e. 3 torr deuterium) is also used in the drift regions.

The characteristics of the magnetic spectrometer are as follows:

1. The drift tube and spectrometer chamber are made from 1/4 in. thick aluminium to shield against external fields and to minimize scattering and X-ray production.
2. Tantalum collimators limit the collected current to a few milliamperes to prevent collective effects from disrupting electron orbits inside the spectrometer.
3. An Armco shield reduces the magnet's fringe field in the collimating region by a factor of 10^{-3}.
4. 10 spectrometer channels are available that cover energies from ~ 10 keV to ~10 MeV for a 200-G field.
5. Faraday cup detectors are used; consequently, time resolution is limited by the bandwidth of the oscilloscope channels (~100 MHz).
6. Time-integrated spectra can also be obtained by appropriate use of the signal cable capacitance.
7. The Faraday cup collectors are situated in the fringe field of the electromagnet to inhibit secondary-electron emission.

The spectrometer was calibrated by mapping the magnetic field produced by the electromagnet with a gaussmeter and using a computer code to follow particle trajectories inside the spectrometer. The error due to the finite width of the collimators is calculated to be about 10%.

An electron beam Faraday cup was used to obtain a direct quantitative measurement of the primary current of the electron beam generated by the plasma focus. Rogowski coils have been used to estimate the magnitude of the electron beam current [36–39], but, because of the plasma return current, interpretation of Rogowski coil signals is not straightforward. Figure 2 shows simultaneous wave forms of Rogowski coil and Faraday cup waveforms. The Faraday cup has a thin mylar window to inhibit the flow of plasma return current.

The electron beam Faraday cup that was built is a slightly modified [4] Pellinen [3] Faraday cup. The cup was designed to measure 100-kA currents, has an experimentally determined [4] bandwidth of 450 MHz, and the 1/4 mil mylar plasma current filter normally

used permits primary electrons with energies down to 27 keV to be collected by the cup.

A solid-state nuclear track detector (SSNTD) technique to measure high fluences of light ions [40] was developed as a means to quantitatively measure the total number of ions accelerated. Fast deuterons striking a converter layer of $Li_2B_4O_7$ interact to produce energetic (d, α) alpha particles which are recorded by a SSNTD placed on the opposite side of the layer. If the shape of the deuteron energy spectrum is known, the track density can be used to estimate the incident beam fluence. The ion energy spectral shape determined by the ion Faraday cup and the observed track density indicate that 1 kJ of the energy deposited in the plasma (~3.8 kJ out of 12.5 kJ) goes into deuterons accelerated to 25 keV or more. The corresponding energy efficiency for this process is about 8%.

The four diagnostics described enable both a qualitative estimate of the electron and ion energy spectra and a quantitative estimate of the total fluence of the beam particles. The results of the experiments using these diagnostics are reported in the next section.

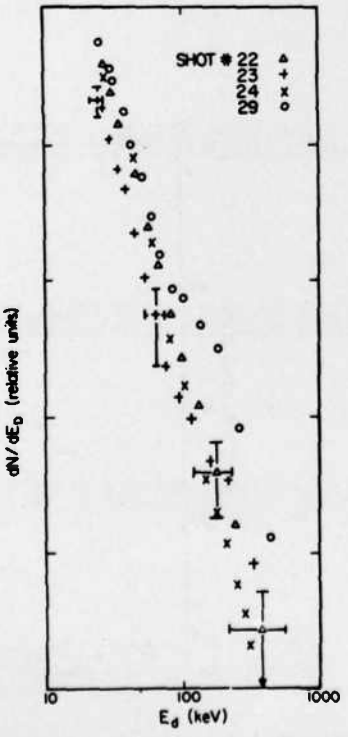

FIG.6. Ion energy spectra from four shots taken on 25 June 1980. Charging voltage on the capacitor bank was 24 kV (11.5 kJ); pressure of deuterium fill gas was 3.0 torr, and neutron yield for all these shots was within 10% of 2.2×10^9.

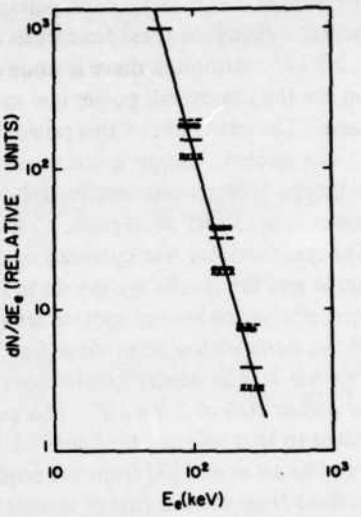

FIG.7. Time-integrated electron beam energy spectra for four separate plasma focus shots taken on 3 Nov. 1980. Data were normalized to lowest energy channel (47 to 74 keV). Charging voltage was 25 kV (12.5 kJ); pressure of deuterium fill gas was 3.0 torr, and neutron yield for all these shots was within 20% of 3.8×10^9.

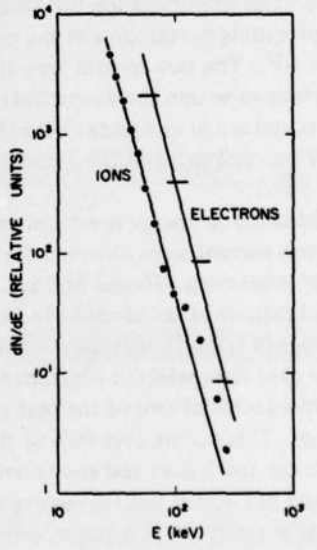

FIG.8. Simultaneously recorded ion and electron energy spectra. Straight lines are power law fits to the ion and electron spectra where exponents are −3.5 and −3.8, respectively.

3. RESULTS

The results of the energy spectra measurements are shown in Figs 6–8. In Fig.6, the ion spectral data for four DPF shots are shown for a deuterium fill gas

pressure of 3 torr and a bank voltage of 24 kV. The neutron yields for these four shots are within 10% of 2.2×10^9. Although there is some evidence of a bump on the tail the overall power law spectra are about the same. The exponent of this power law is -3.4 ± 0.4.

The electron energy spectra were measured with the magnetic spectrometer for four shots under similar conditions (3 torr deuterium, 25 kV bank voltage). The spectrometer was operated in the time-integrated mode and the results are shown in Fig.7. As with the ions, power-law energy spectra are observed on each of the shots with a mean value for the exponent of -3.6 ± 0.3. The neutron yields for these four shots lie within 20% of 3.8×10^9. This power law is equivalent to that inferred by Lee et al. [16] and Van Paasen et al. [18] from the hard X-ray spectra emitted from plasma foci of similar energies and neutron yields. It is also interesting that this same spectrum of hard X-rays was observed during the reconnection phase of a double inverse pinch [41], possibly indicating a similar process in a device of quite different geometry.

The results of a simultaneous observation of the electron and ion beam energy spectra are shown in Fig.8. The conditions are the same as described in the preceding paragraph and the neutron yield was 3.4×10^9. The two spectra have the same power law structure to within the uncertainty in the measurements and are in agreement with the results of the other measurements at these conditions shown in Figs 6 and 7.

The electron energy spectrum and total primary electron current were observed for main bank currents between 350 and 560 kA. To avoid the complications of radial spoke formation and parasitic currents [42] which may vary from shot to shot only those data were selected which had a neutron yield within a factor of two of the best yield at that bank voltage. This occurs over 60% of the time at 25 kV where the spark gaps and anode length are more optimal but occurs less frequently when the bank voltage is reduced. It is assumed that the effects of parasitic current formation are minimal at high neutron yields (there is no neutron yield when radial spokes form [42]) and the peak yield scales as the $I_{MB}^{4.4 \pm 0.3}$ for the Illinois plasma focus (Fig.5), a dependence reported by several other investigators when the performance of their plasma focus devices is optimal [43].

The electron magnetic spectrometer was operated as shown in Fig.4. The perpendicular magnetic field was nominally at 200 G and six energy channels were used, spanning a mean energy range between 30 and 400 keV.

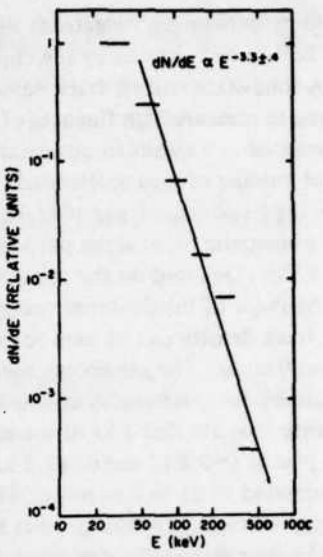

FIG.9. Typical time-integrated electron energy spectrum observed with electron magnetic spectrometer (see Fig.4) for $I_{MB} = 560$ kA. Filling pressure was 3 torr deuterium; bank voltage was 25 kV ((1/2) $CV^2 = 12.5$ kJ).

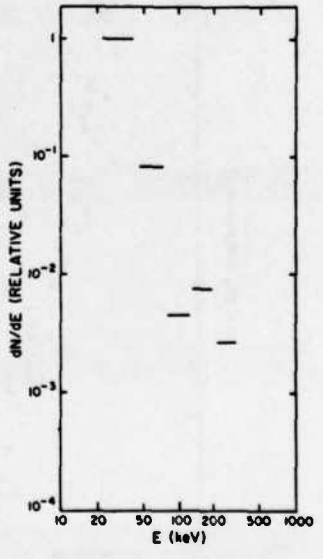

FIG.10. Typical time-integrated electron energy spectrum observed with the electron magnetic spectrometer (see Fig.4) for $I_{MB} = 370$ kA. Filling pressure was 3 torr deuterium; bank voltage was 17.5 kV ((1/2) $CV^2 = 6.1$ kJ).

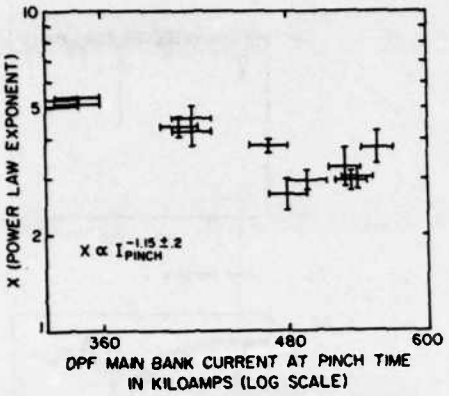

FIG.11. Observed scaling of the power law exponent, $x(dN/dE \propto E^{-x})$, with I_{MB}. Filling pressure was 3 torr deuterium; vertical error bars represent least-square error in power law slopes for various observations.

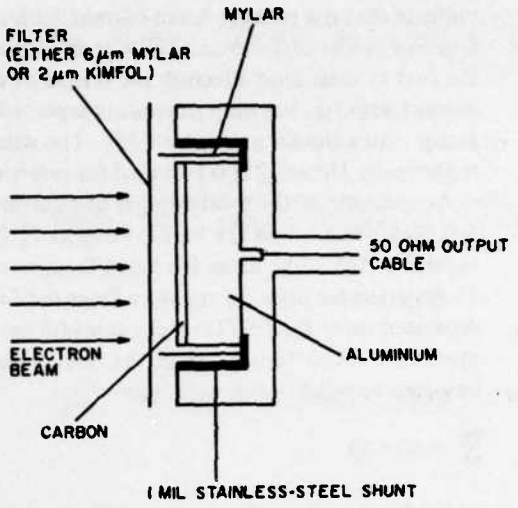

FIG.12. Schematic view of high-current fast Faraday cup used to measure primary electron current. Areas behind filter are evacuated to about 0.04 torr to increase voltage stand-off.

As above, power law energy spectra were observed for the electrons (Fig.9) although bumps-on-the-tail of the energy distributions were sometimes observed at lower bank currents (Fig.10). Since the bump formation process appears to be different from the power law formation process [44] and is intermittent, these bumps were not included in calculating power law exponents. The results are shown in Fig.11. The electron spectra appear to harden with increasing I_{MB} where the absolute value of the exponent, $|x|$, scales as $I_{MB}^{-1.15\pm0.2}$. These results are consistent with the hard-X-ray data where the absolute value of the electron beam energy power law ranged from 3.5–4.0 for 20 kJ devices [16, 18] to 2.4–4.0 for a 57.3 kJ device [17], and down to 2.0 for a 375 kJ device [19]. Thus the results from the 6–12.5 kJ device reported here fit these X-ray data fairly well although these new results are less ambiguous, being the result of a direct measurement.

The fill pressure for the DPF for all the data reported here is 3 torr D_2. However, varying the pressure between 2 and 4 torr at a bank voltage of 25 kV ($I_{MB} \sim 560$ kA) had no effect on the power law (-3.4 ± 0.4) although the signals were stronger at 2 torr and weaker at 4 torr.

The scaling of the peak in the primary current with I_{MB} was also determined. The electron magnetic spectrometer (Fig.4) was replaced by the electron Faraday cup (Fig.12) to measure the primary current of the electron beam. The filter had to be replaced after each shot and so a gate valve was inserted into the drift tube and opened after the plasma focus had been conditioned.

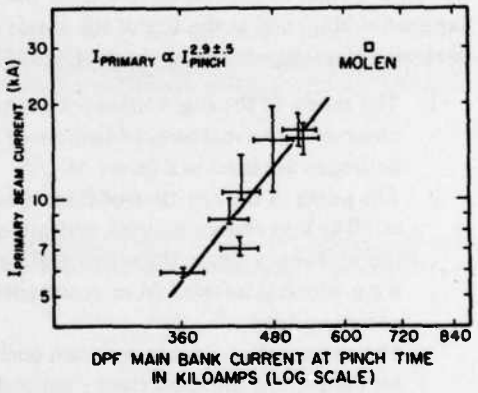

FIG.13. Observed scaling of peak primary current (first peak in top trace of Fig.2) with I_{MB}. Filling pressure was 3 torr deuterium.

Typical data are shown in Fig.2 where the Rogowski coil signal (net current) is included for reference. When the filter is removed, the Faraday cup signal closely follows the form of the Rogowski coil signal although reduced by about 15%, presumably because of beam divergence. The difference between these two signals illustrates the difficulty in interpreting Rogowski coil signals caused by these electron beams which have been reported in the past [36–39].

The results of the scaling measurements for the primary beam current are shown in Fig.13. The data

indicate that the primary beam current increases with I_{MB} to a power of 2.9±0.5. These measurements are the first of their kind although the scaling of the net current with I_{MB} has been previously reported by this group with a similar power law [39]. The data point reported by Molen [21] is included for reference.

An estimate of the total number of electrons in the fast peak observed on the Faraday cup at 12.5 kJ is of order 2×10^{15}. The mean ion beam fluence over a 15-cm-diameter plate 20 cm away from the focus estimated using the SSNTD technique [40] for a similar shot is $6 \pm 2 \times 10^{14}\,cm^{-2}$. Since the track density is observed to be uniform, we obtain

$$\frac{N_+}{N_e} \sim 50 \pm 30$$

where N_+ and N_e are the numbers of ions and electrons accelerated, respectively. The ratio is of order $(M_+/M_e)^{1/2}$, which is predicted by a model for a uniform-current-density diode accelerator [45].

The assumptions that fast deuterons are created at the same instant as the fast electrons (or the X-ray bremsstrahlung) and at the top of the anode are consistent with three experimental observations [5].

1. The ratios of the flight times for the two peaks observed when mixtures of deuterium and hydrogen are used as a factor of $\sqrt{2}$.
2. The peaks in the raw time-of-flight data occur at 80 keV as consistent with multiple-scattering theory [46] in 3 torr D_2 with a path length of 6 cm which is inferred from geometrical considerations.
3. The measured secondary-emission coefficient for copper has the same energy dependence as that observed in dedicated experiments [47].

Since these observations involve independent phenomena the self-consistency is fairly solid evidence for the simultaneous creation of the two species within experimental uncertainties (±2cm, ±5 ns).

Figures 14 and 15 show that the fast electrons as evidenced by the 100-keV channel of the electron magnetic spectrometer and the hard-X-ray bremsstrahlung peak on our plastic scintillator-photomultiplier tube occur simultaneously with a peak in $|\dot{I}|$. The bremsstrahlung peak occurs at the second and slightly smaller $|\dot{I}|$ peak (Fig.15) and this may indicate a change in sign in $\dot{L}$ [29].

Figure 16 shows the magnitude of the terms not involving $\dot{L}(V = q/C + L\dot{I})$ estimated for $I_{MB} = 560$ kA. To compare this with the maximum (E_M) energy of the particles accelerated, the maximum-energy channel

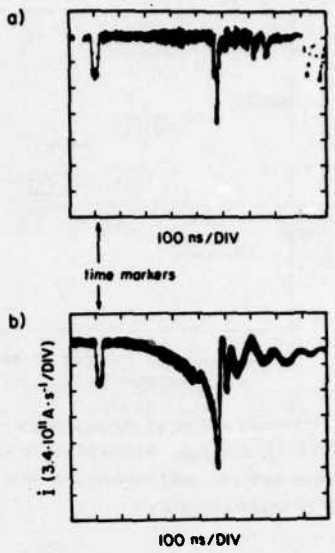

FIG.14. Simultaneous waveforms of a) 100-keV (±20 keV) channel of electron magnetic spectrometer and b) $\dot{I}$-waveform of the mainbank current. Filling pressure was 3 torr deuterium; bank voltage was 25 kV.

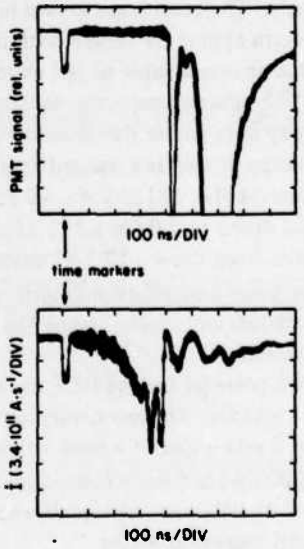

FIG.15. Simultaneous waveforms of a) scintillator photomultiplier tube and b) $\dot{I}$ waveform of main bank current. Long narrow peak in a) has been identified as hard-X-ray bremsstrahlung produced by the fast electrons in the beam and the broader second peak as the neutrons produced by the device. Waveform a) is delayed 40 ± 4 ns with respect to b), due to inherent delay of photomultiplier tube, differences in cable length and time-of-flight. Filling pressure was 3 torr deuterium; bank voltage was 25 kV.

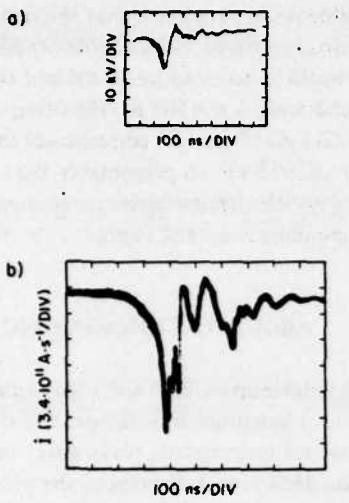

FIG.16. Typical waveforms of a) voltage across the capacitor bank (q/C) and b) $\dot{I}$ of the mainbank current (the two peaks are simultaneous). These waveforms can be used to calculate two of the three terms of the possible accelerating voltage across the plasma diode (excluding the $L\dot{I}$ term). The circuit inductance at pinch time is estimated to be 50 nH on the basis of time-integrated pin-hole camera pictures so the total of q/C and $L\dot{I}$ is 110 kV. (The base line in a) is one division below the top.)

receiving signal is the 400-keV channel. Thus, the 110 keV estimated in Fig.16 is only about one fourth of E_M. Evidence from measurements using solid-state nuclear track detectors [40] indicates that some deuterons acquire an energy greater than 1.0 MeV Particles with energies from 1–5 MeV have been observed in several other DPF devices [6–8, 11–15].

4. DISCUSSION

The results reported in Section 3 have implications on two aspects of DPF phenomena:

1. the neutron production mechanism, and
2. the acceleration mechanism.

These aspects will be treated in this section.

Since the total number of particles accelerated and their energy spectra have been determined one can use this information to predict the magnitude and the scaling of the axial beam target neutron yield with I_{MB} if a few simple assumptions are made about the target. If the target is assumed to be the cold gas ahead of the beam then it is independent of bank parameters.

TABLE I. THEORETICAL AND EXPERIMENTAL DATA

Phenomena	Experiment	Cold target	Hot target
$Y_n \propto I_{MB}$, X	4.6 ± 0.3	5.2 ± 1.0	4.8 ± 1.0
Target thickness		15 cm, 3 torr	2.9×10^{18} deuterons·cm^{-2}
Y_n at 12.5 kJ	3.8×10^9	2.4×10^9	3.1×10^9
Anisotropy ($Y_{n0°}/Y_{n90°}$)	1.5	2.2	1.7
Neutron pulse width at 3.2 m	90 ns	60 ns*	30 ns*

* Assumes axial beam motion only and includes 20-ns pulse width

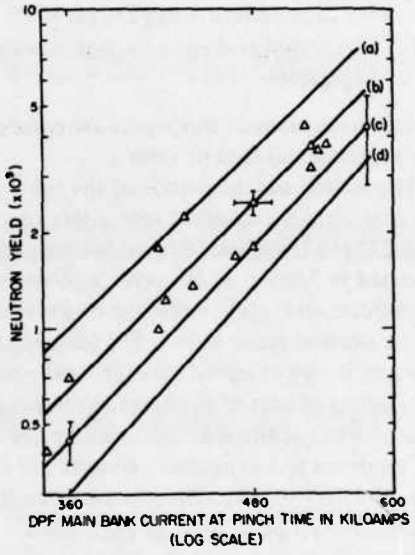

FIG.17. Neutron yield in Illinois plasma focus and predictions of various models:

- *i) Curve a) is least-square fit to peak neutron yield versus I_{MB} ($Y_n \propto I_{MB}^{4.4\pm0.3}$).*
- *ii) Curve b) is least-square fit to neutron yield for shots actually used to determine the data in Figs 11 and 13. Triangles are data with representative error bars shown for one of the points. For these data $Y_n \propto I_{MB}^{4.6\pm0.3}$.*
- *iii Curve c) is result of beam hot target model for a target thickness of 2.9×10^{18} deuterons·cm^{-2}. Error bars are those associated with experimental uncertainties in the beam parameters shown in Figs 11 and 13. The model predicts $Y_n \propto I_{MB}^{4.8}$.*
- *iv) Curve d) is result of beam cold gas target for a target of 3 torr deuterium gas 15 cm long (target thickness 2.9×10^{18} deuterons·cm^{-2} as in iii) where effects of slowing-down on deuteron beam have been included. Error bars are as in iii) and this latter model predicts $Y_n \propto I_M^{5.2}$.*

Similarly, if one assumes a hot target (plasma) of density and length independent of I_{MB}, which is roughly consistent with several experiments [48–52], even slowing-down of the deuterons could be neglected for $T_e > 500$ eV for targets less than 10 cm in length. Thus in calculating the axial-beam target neutron yield the following assumptions have been made:

1. The ion beam energy spectrum has the same power law dependence as the electron beam energy spectrum for a given I_{MB}.
2. $N_i/N_e = (M_i/M_e)^{1/2}$.
3. The ion and electron energy beam spectra are the same at all angles to the axis where the beams exist.
4. The target parameters are independent of I_{MB}.
5. The slowing-down in the cold gas target is that for deuterons in 3 torr D_2 gas [53].
6. The slowing-down in the hot plasma target is negligible.

The predictions of this model are compared with the experimental data in Table I.

The scaling and magnitude of the beam target neutron yield is consistent with either target model (Fig.17) and the electron beam scaling parameters reported in Section 3. However, neither target model is adequate to explain either the observed anisotropy or the neutron pulse width. The long pulse width and low anisotropy observed experimentally could be due to trapping of part of the beam in some magnetic structure of the focus as evidenced by the high ratio of DT neutrons to DD neutrons observed in other DPF experiments [50, 54]. Description of such trapping is beyond the scope of these target models.

Owing to the assumptions made in the calculations, the agreement in the magnitude and scaling of the beam target model prediction of neutron yield and the experimental result only means that the axial beam target model cannot be ruled out. Probably the most questionable assumption is that the deuteron beam energy spectrum is the same at all angles (to 15°) with respect to the device axis. This is apparently true for the electron beam which is not always on axis (presumably because of the frozen-hose instability [55]) and yet always gives the same power law spectrum (within the error). The large uniform patterns of tracks observed in the SSNTD converter layer technique [40] (which has a lower energy threshold of about 150 keV) over a 19° angle with respect to the axis also support the assumption. And, finally, the deuteron energy spectra are roughly independent of the angle for a 28-kJ DPF at 5 torr D_2 in the energy range from 0.9 to 4.5 MeV [52].

One possible paradox is that the instantaneous ion current is estimated to be $eN_i/\Delta t \sim 800$ kA (where the pulse width is taken to be 20 ns) and the peak device current is only 5.6×10^5 A. However, the mean ion speed (2.1×10^8 cm·s^{-1}) corresponds to an electron energy of ~13 eV, so presumably the ions drag along low-energy electrons which cancel any net current and corresponding magnetic energy.

ACCELERATION MECHANISM

It is clear from Figs14 and 15 that the electron (and hence ion) beam occur at the peak in $|\dot{I}_{MB}|$, indicating that current interruption plays a role in the acceleration process. However, estimates of the induced voltage across the pinch from the observed voltage surge across the parallel-plate transmission lines between the capacitor banks and the DPF device and $L\dot{I}$ (where L is estimated from pinhole camera pictures) indicate that only about 100 kV appears across the pinch due to $|\dot{I}_{MB}|$ phenomena. This voltage is much too low to explain the high particle energies observed by simple diode acceleration if current interruption ($\dot{I}$) was the only source of the applied potential.

It has been suggested [56] that motion of the current sheath could cause induced voltages much higher than $L\dot{I}$ effects and the computational results of Kondoh and Hirano [29] contain estimates of the magnitude of this effect. The system of equations used by the latter authors has been programmed and used to estimate the induced voltage for the Illinois DPF device. The final radial collapse ($r_0 = 2.5$ cm) was modelled and the initial conditions were determined experimentally by placing a co-axial short across the open end of the plasma focus electrode and measuring the circuit characteristics when the device was evacuated. At 3 torr D_2 pressure, the code estimates total induced voltages range up to ~ 100 kV for a peak device current of 560 kA. Hence it appears that even sheath motion cannot provide sufficient potentials to explain the observed particle energies (which apparently range above 1 MeV in this device [40]) by the simple process of diode acceleration.

CONCLUSIONS

The energy spectra of the fast ions and electrons emitted by the plasma focus in opposite directions (Fig.1) are observed by direct methods to have the same power law energy dependence at a device current at pinch time, I_{MB}, of 560 kA. The scaling of the

absolute value of the exponent of the power law was found (for electrons) to decrease with increasing I_{MB} (hardening of the spectrum) and the values were found to be consistent with the electron energy spectra inferred from hard X-ray spectral measurements on several other devices [16–19]. It is interesting that power law spectra of similar exponents have also been observed in a double inverse pinch [41], cosmic rays [57], and solar flares [58].

The magnitude of the fast electron current has been measured by a filtered fast Faraday cup and found to scale as I_{MB} to the third power. The highest primary beam current observed was 17 kA for a bank energy of 12.5 kJ. Since much more energetic plasma foci exist such as the 1 MJ device at Frascati [50], it would be very interesting if similar measurements were performed on these devices to see if the scaling observed in the Illinois device persists at high bank energy. If so, the hardening of the energy spectra indicated by these measurements and others [16–19] may lead to new applications of the DPF as a pulsed electron beam source.

The measured beam parameters and scaling laws can be used to predict the scaling and magnitude of the neutron yield due to a beam target model. If the target parameters are assumed to be independent of I_{MB}, then the agreement between beam target yield and the observed yield is quite good with respect to scaling and magnitude but the predictions of the model do not fit the observed temporal neutron pulse width and anisotropy. It is possible that trapping of all or part of the deuteron beam by magnetic structures in the plasma focus [50] could explain the latter discrepancies.

The beams are observed to occur at the peak in the current interruption ($\dot{I}_{MB}$), indicating that it has a strong influence on the acceleration process but the magnitudes of the voltages generated by d/dt (LI) effects estimated from circuit measurements are too low to explain the acceleration process by simple diode acceleration.

ACKNOWLEDGEMENTS

The authors wish to thank Drs J.H. Lee, S. Graybill and K.G. Tirsell for helpful discussions and H.L. Stalker and C. Luesse for fabricating the magnetic spectrometer. The loan of the electromagnet for the spectrometer by Argonne National Laboratory is gratefully acknowledged as is the loan of the DPF capacitor bank from NASA Langley. This research was supported in part by the Air Force Office of Scientific Research, Contract No.AFOSR-79-0121.

REFERENCES

[1] MATHER, J.W., Dense Plasma Focus, in Methods of Experimental Physics 9, Part B, Academic, New York (1971) 210.
[2] ALFVÉN, H., CARLQVIST, P., Solar Phys. 1 (1967) 220; CARLQVIST, P., Solar Phys. 7 (1969) 377.
[3] PELLINEN, D., Rev. Sci. Instrum. 41 (1970) 1347.
[4] STYGAR, W.A., Ph. D. Thesis, Univ. of Illinois, Urbana-Champaign (May 1982).
[5] GERDIN, G., STYGAR, W., VENNERI, F., J. Appl. Phys. 52 (1981) 3269.
[6] GULLICKSON, R.L., SAHLIN, H.L., J. Appl. Phys. 49 (1978) 1099.
[7] FILIPPOV, N.V., FILIPPOVA, T.I., JETP Lett. 25 (1977) 241.
[8] BERTALOT, L., BILBAO, L., BRUZZONE, H., GENTILINI, A., GOURLAN, C., GULLICKSON, R.L., KROEGLER, H., PODDA, S., RAGER, J.P., ROBOUCH, V.B., STEINMETZ, K., in Controlled Fusion and Plasma Physics (Proc. 9th Europ. Conf. Oxford, 1979) Vol.1 (1979) 108.
[9] KROMPHOLZ, H., MICHEL, L., SCHÖNBACH, K.H., FISCHER, Heinz, Appl. Phys. Lett. 13 (1977) 29.
[10] VASILEVA, R.P., PERGAMENT, M.I., YAROSLAVSKY, A.I., Nucl. Fusion Special Suppl. (1969) 129.
[11] GULLICKSON, R.L., McCLURE, J.W., PICKLES, W.L., PRICE, D.F., WAINWRIGHT, T.E., WILLIAMS, M.D., 1980 IEEE Int. Conf. on Plasma Sci. Conf. Record – Abstracts, IEEE Catalog No.80 CH1544-6 NPS (1980) 75.
[12] KITAGAWA, Y., YAMADA, Y., ISHIZAKI, A., NAITO, M., YOKOYAMA, M., YAMANKA, C., ibid., 74.
[13] RHEE, M.J., Appl. Phys. Lett. 37 (1980) 906.
[14] HEROLD, H., MOZER, A., SADOWSKI, M., SCHMIDT, H., Rev. Sci. Instrum. 52 (1981) 24.
[15] BELYAEVA, I.F., Nucl. Fusion 20 (1980) 1037.
[16] LEE, J.H., LOEBBAKA, D.S., ROOS, C.E., Plasma Phys. 13 (1971) 347.
[17] GULLICKSON, R.L., BARLETT, R.H., Adv. X-ray Anal., 18 (1971) 184.
[18] VAN PAASEN, H.L.L., VANDRE, R.H., WHITE, R.S., Phys. Fluids 13 (1970) 2606.
[19] JOHNSON, D.J., J. Appl. Phys. 45 (1974) 1147.
[20] WAINWRIGHT, T., PICKLES, W., McCLURE, J., PRICE, D., ELTGROTH, P., Results of the LLNL Plasma Focus Project, Preprint UCID-19175 (1981).
[21] MOLEN, G.M., in Energy Storage, Compression and Switching (Proc. 2nd Int. Conf. Venice, Italy, 1978) Plenum Press.
[22] HIRANO, K., KONDOH, Y., SHIMODA, K., YAMAMOTO, T., 1981 IEEE Int. Conf. on Plasma Sci., Conf. Record-Abstracts, IEEE Catalog No.81CH1640-2 NPS (1981) 120.

[23] NARDI, V., BOSTICK, W.H., FEUGEAS, J., PRIOR, W., Phys. Rev. A 22 (1980) 2211.
[24] GRAYBILL, S.E., IEEE Trans. Nucl. Sci. NS-18 (1971) 438.
[25] KOTLYAREVSKII, G.I., USOV, Yu.P., Sov. Phys. Tech. Phys. 21 (1976) 887.
[26] VERNON, M.E., M.S. thesis, University of Illinois (1979).
[27] BAÑUELOS, A., BRUZZONE, H., DELELLIS, R., GRATTON, J., GRATTON, R., KELLY, H., MILANESE, M., POUZO, J., RODRIGUEZ-TRELLES, F., in Plasma Physics and Controlled Nuclear Fusion Research (Proc. 7th Int. Conf. Innsbruck, 1978) Vol.2, IAEA, Vienna (1979) 173.
[28] STYGAR, W.A., M.S. thesis, University of Illinois (1980).
[29] KONDOH, Y., HIRANO, K., Phys. Fluids 21 (1978) 1617.
[30] GOLDSTEIN, S.A., LEE, R., Phys. Rev. Lett. 35 (1975) 1079.
[31] YONAS, G., SPENCE, P., PELLINEN, D., ECKER, B., HEWILIN, S., Dynamic Effects of High ν/γ Beam Plasma Interactions, Physics International Report PITR-106-1, San Leandro, California (1969).
[32] YONAS, G., SPENCE, P., ECKER, B., RANDER, J., Dynamic Effects of High ν/γ Beam Plasma Interaction, Physics International Report PIFR-106-2, San Leandro, California (1969).
[33] MILLER, P.A., GERARDO, J.B., POUKEY, J.W., J. Appl. Phys. 43 (1972) 3001.
[34] MILLER, P.A., GERARDO, J.B., J. Appl. Phys. 43 (1972) 3008.
[35] KOTLYAREVSKII, G.I., USOV, Yu.P., Sov. Phys. Tech. Phys. 23 (1978) 289.
[36] BOSTICK, W.H., NARDI, V., PRIOR, W., FEUGEAS, J., KILIO, H., POWELL, C., Bull. Amer. Phys. Soc. 23 (1978) 848.
[37] GERDIN, G., STYGAR, W., VERNON, M., 1979 IEEE Int. Conf. on Plasma Sci., Conf. Record-Abstracts, IEEE Catalog No.79 CH1410-0 NPS (1979) 111.
[38] STYGAR, W., GERDIN. G., Bull. Am. Phys. Soc. 24 (1979) 1039.
[39] GERDIN, G., STYGAR, W., VENNERI, F., 1980, IEEE Int. Conf. on Plasma Sci., Conf. Record-Abstracts IEEE Catalog No.80 CH1544-6 (1980) 75.
[40] GERDIN, G., DURHAM, J., ILIĆ, R., Nuclear Tracks 5 (1981) 299.
[41] BAUM, P.J., BRATENAHL, A., WHITE, R.S., Phys. Fluids 16 (1973) 226.
[42] OPPENLÄNDER, T., PROSS, G., DECKER, G., TRUNK, M., Plasma Phys. 19 (1977) 1075.
[43] MATHER, J.W., Methods of Experimental Physics 9B Academic Press (1971) 187.
[44] PICKLES, W., private communication.
[45] HOHL, F., GARY, S.P., Phys. Fluids 20 (1977) 683.
[46] ROSSI, B., GREISEN, K., Rev. Mod. Phys. 13 (1941) 240; EYGES, L., Phys. Rev. 74 (1948) 1534.
[47] HILL, A.G., BUECHNER, W.W., CLARK, J.S., FISK, J.B., Phys. Rev. 55 (1939) 463.
[48] FORREST, M.J., PEACOCK, N.J., Plasma Phys. 16 (1974) 489.
[49] BERNARD, A., COUDEVILLE, A., JOLAS, A., LAUNSPACH, J., DeMASCUREAU, J., Phys. Fluids 18 (1975) 180.
[50] RAGER, J.P., Progress on Plasma Focus Research at Frascati, C.N.E.N. Report 81.43/cc C.N.E.N.-Edizioni Scientifiche C.P. 65 00044 Frascati Rome, Italy (Sept. 1981).
[51] HIRANO, K., SHIMODA, K., HAMADA, F., Jpn. J. Appl. Phys. 17 (1978) 1619.
[52] SCHMIDT, H., Atomkernenergie-Kerntechnik 36 (1980) 161.
[53] ANDERSEN, H.H., ZIEGLER, J.F., Hydrogen Stopping Power and Ranges in all Elements: Stopping and Ranges of Ions in Matter, Vol.3, Pergamon Press, New York (1977).
[54] HÜBNER, K., STEINMETZ, K., RAGER, J.P., ROBOUCH, B.V., 1981 IEEE Int. Conf. on Plasma Sci., Conf. Record-Abstracts, IEEE Catalog No.81 CH1640-2 NPS (1981) 59.
[55] PUTNAM, S., Transverse Instabilities of Intense, Relativistic Electron Beams, PIIR-7-68, Physics International Co., San Leandro, CA (March 1968).
[56] NEWMAN, C.E., PETROSIAN, V., Phys. Fluids 18 (1975) 547.
[57] ROSSI, B., Cosmic Rays, McGraw-Hill, New York (1964) 174.
[58] RAMATY, R., COLGATE, S.A., DULK, G.A., HOYNG, P., KNIGHT, J.W., LIN, R.P., MELROSE, D.B., ORRALL, R., PAIZIS, C., SHAPIRO, P.R., SMITH, D.F., Van HOLLEBEKE, M., Energetic Particles in Solar Flares, in Solar Flares (STURROCK, P.A., Ed.), Colorado Assoc. Univ. Press, Boulder, CO (1980) 117.

(Manuscript received 28 July 1981
Final manuscript received 16 July 1982)

END

FILMED

5-85

DTIC

have applications to astrophysics as well.

† This article is based on a portion of the PhD thesis submitted by one of the authors (WS) in partial fulfilment of the requirements for the doctoral degree at the University of Illinois.

* Present address: Sandia National Laboratory, Albuquerque, New Mexico, 87185, USA.

Figure 2 illustrates that current interruption is a source of energy in a plasma focus. The lowest trace is the main bank current waveform of the plasma focus. The sharp reduction in the current by a factor of two at pinch time indicates [1] that one-half the magnetic energy was coupled into the pinch (i.e. 3.8 kJ).

spectra of ions and electrons emitted from a plasma focus are reported. Also the scaling of the primary electron beam current and energy spectrum with the total DPF main bank current at pinch time, I_{MB}, are reported for the first time [4]. The ions and electrons are accelerated in the directions shown in Fig. 1. The ion beam energy spectra were measured with a Faraday

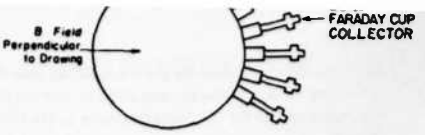

FIG. 4. Schematic view of electron magnetic spectrometer.

permit direct observation of fast particles emitted from the lower end of the pinch. The outer diameter of the centre electrode is 5.08 cm and the inner diameter of the squirrel cage (outer electrode) is 10.2 cm. The centre electrode extends 14 cm beyond a lavite insulator [26]. The electrode material is OFHC copper; there is evidence that oxygen released from regular

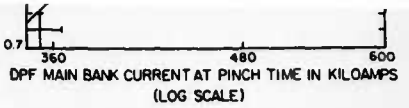

FIG.5. Plot of neutron yield versus plasma focus current at pinch time. Filling pressure was 3 torr deuterium; bank voltage range 16–24 kV.

used previously to transport electron beams (with $\nu/\gamma \ll 1$ and $\nu/\gamma \approx 1$) with less than 20% loss of beam charge over distances of ~ 1 m at optimum pressure [31, 32]. The optimum pressure is defined to be that pressure at which the electron beam charge is transported with minimum loss [33, 34], and is also the return current.

The electron beam Faraday cup that was built is a slightly modified [4] Peilinen [3] Faraday cup. The cup was designed to measure 100-kA currents, has an experimentally determined [4] bandwidth of 450 MHz, and the 1/4 mil mylar plasma current filter normally

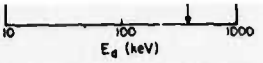

FIG.6. Ion energy spectra from four shots taken on 25 June 1980. Charging voltage on the capacitor bank was 24 kV (11.5 kJ); pressure of deuterium fill gas was 3.0 torr, and neutron yield for all these shots was within 10% of 2.2×10^9.

3. RESULTS

The results of the energy spectra measurements are shown in Figs 6–8. In Fig.6, the ion spectral data for four DPF shots are shown for a deuterium fill gas

their plasma focus devices is optimal [43].

The electron magnetic spectrometer was operated as shown in Fig.4. The perpendicular magnetic field was nominally at 200 G and six energy channels were used, spanning a mean energy range between 30 and 400 keV.

FIG.10. Typical time-integrated electron energy spectrum observed with the electron magnetic spectrometer (see Fig.4) for I_{MB} = 370 kA. Filling pressure was 3 torr deuterium; bank voltage was 17.5 kV ((1/2) CV^2 = 6.1 kJ).

of the electron beam. The filter had to be replaced after each shot and so a gate valve was inserted into the drift tube and opened after the plasma focus had been conditioned.

signals caused by these electron beams which have been reported in the past [36–39].

The results of the scaling measurements for the primary beam current are shown in Fig.13. The data

involving $\dot{L}(V = q/C + L\dot{I})$ estimated for $I_{MB} = 560$ kA. To compare this with the maximum (E_M) energy of the particles accelerated, the maximum-energy channel

Waveform a) is delayed 40 ± 4 ns with respect to o), due to inherent delay of photomultiplier tube, differences in cable length and time-of-flight. Filling pressure was 3 torr deuterium; bank voltage was 25 kV.

if a few simple assumptions are made about the target. If the target is assumed to be the cold gas ahead of the beam then it is independent of bank parameters.

slowing-down on deuteron beam have been included. Error bars are as in iii) and this latter model predicts $Y_n \propto I_M^{5.2}$.